geosciences

MDPI

Article

Remote Sensing and GIS Contribution to a Natural Hazard Database in Western Saudi Arabia

Barbara Theilen-Willige [1,*] and Helmut Wenzel [2]

1 Institute of Applied Geosciences, Technische Universität Berlin (TU Berlin), D-10587 Berlin, Germany
2 Wenzel Consulting Engineers GmbH, 1180 Vienna, Austria
* Correspondence: Barbara.Theilen-Willige@t-online.de

Received: 14 August 2019; Accepted: 27 August 2019; Published: 31 August 2019

Abstract: The most frequent disasters in Western Saudi Arabia are flash floods, earthquakes and volcanism, especially submarine volcanism potentially causing tsunamis in the Red Sea and submarine mass movements, dust storms and droughts. As the consequences and effects of the climate change are expected to have an increasing impact on the intensity and occurrence of geohazards as flash floods, length of drought periods, or dust storms, the systematic, continuous monitoring of these hazards and affected areas using satellite data and integration of the results into a geographic information systems (GIS) database is an important issue for hazard preparedness and risk assessment. Visual interpretation and digital image processing of optical aerial and satellite images, as well as of radar images, combined with Advanced Spaceborne Thermal Emission and Reflection Radiometer (ASTER), Shuttle Radar Topographic Mission (SRTM) and Advanced Land Observing Satellite (ALOS) PALSAR DEM data are used in this study for the mapping and inventory of areas prone to geohazards, such as flash floods or tsunami flooding. Causal or critical environmental factors influencing the disposition to be affected by hazards can be analyzed interactively in a GIS database. How remote sensing and GIS methods can contribute to the detection and continuously, standardized monitoring of geohazards in Western Saudi Arabia as part of a natural hazard geodatabase is demonstrated by several examples, such as the detection of areas prone to hydrological hazards, such as flash floods causing flooding of roads and settlements, the outlining of coastal areas of the Red Sea prone to tsunami flooding and storm surge, the mapping of traces of recent volcanic activity, and of fault/fracture zones and structural features, especially of ring structures.

Keywords: W-Saudi Arabia; natural hazards; remote sensing; GIS

1. Introduction

Western Saudi Arabia is prone to different natural hazards, such as earthquakes, tsunamis, slope failure and volcanic hazards, as well as flash floods after heavy rainfalls. Slope failure, especially rock fall, is a common phenomenon in the mountainous regions. Hazards in these arid areas include increased erosion, salinization, shifting sand dunes and dust storms [1]. Over the last decades, floods have been the most recurrent disasters recorded in the Emergency Events Database (EM-DAT) [2], followed by earthquakes, storms and droughts, indicating a strong need for early warning systems and disaster risk management. The low percentage for droughts listed in the EM-DAT is due to limited data availability.

As the consequences and effects of the climate change will have an increasing impact on the intensity and occurrence of natural hazards, such as flash floods, length of drought periods, or storms [3], the surveillance and systematic, continuous monitoring of these hazards is an important issue.

Further on the human impact on the landscape has to be considered (increasing of built areas, mining, more intensified land use). The increase of the built environment and the enlargement of urban areas has led to a great impact on the landscape and susceptibility to natural hazards.

Web geographic information systems (GIS) and modern mobile personal computing technologies enable public access to up to date land images and spatial data of the highest possible resolution, available to everybody. Many countries and organizations have developed, such as public available, operational working national natural hazard database services, such as the Natural Hazard Viewer of National Oceanic and Atmospheric Administration (NOAA), including interactive web map services providing information on the regional, different natural hazards and disaster management [4]. Another example is Bhuvan, the Indian Geo-Platform, integrating satellite and natural hazard data combined with infrastructural data and additional thematic layers [5]. Meanwhile, the use of earth observation (EO) products and geographic information systems (GIS) has become an operational working approach in disaster-risk assessment and management [6,7]. Similar efforts are supported in Saudi Arabia and are in the process of construction [8]. However, open data access and interactive Web-GIS maps in environmental applications, especially focusing on the management of natural hazards, are still in development in Saudi Arabia. It requires the processing of all available data from different sources depending on the type of hazard and the local characteristics. Standardization is a known issue in open data, which is very important to achieve interoperability. Proprietary rights, formats, legacy data, transition costs, the huge diversity of data sources, or any other limitation, still form hindrances to the standardized data [9]. The procedure and focus of the data mining should be adapted to the specific characteristics, needs, priorities and hazard occurrence in this country. This paper might be a contribution to show ways and workflows that could be useful for the implementation of such a Web GIS.

An overview of the different natural hazards in Western Saudi Arabia is given in the next chapter.

2. Overview of Natural Hazards in Western Saudi Arabia

2.1. Flash Floods

In the arid areas of western Saudi Arabia, flash floods are generated after high-intensity rainfall events, particularly on steep mountainous terrain and hilly slopes that are barren and lack vegetation cover. Flash floods and associated debris flows are quite common along the steeper slopes and valleys of the western escarpments [10] during the wetter season. The runoff generated during the occasional heavy rainstorms in the region, coupled with urban growth are the main causes of the occurrence of flash floods. Though the average annual rainfall in Saudi Arabia is only about 100 mm, hydro-logical hazards occur especially in the big cities like Jeddah and Makkah, mainly due to rapid urbanization which has led to the development of housing in topographically low-lying regions and obstruction of the natural drainage systems. The urbanization significantly decreases the permeability of the soil and, thus, leads to a crucial increase in hazardous water surface runoff [11].

2.2. Earthquake Hazard

The general physiography of western Saudi Arabia is characterized by the Red Sea coastal plains and the escarpment foothills called Tihama. Along this zone, sabkha areas exist in longitudinal stretches parallel to the shoreline of the Red Sea [10]. The Arabian Peninsula forms a tectonic plate surrounded by active boundaries with earthquake occurrence [12]. Following the rifting of the Red Sea Basin some 30 million years ago, the Red Sea region became a broad zone of active deformation between Africa and Arabia. Seismicity in the region is caused by the collision of the Arabian plate with the Eurasian plate along the Zagros and Bitlis thrust system, rifting and seafloor spreading in the Red Sea and the Gulf of Aden. A concentration of earthquake activities is monitored along the Red Sea Rift and the Gulf of Aqaba [1,13].

The Red Sea is a narrow ocean basin, separating the African plate from the Arabian plate. It is approximately 3000 km long and about 100 to 300 km wide. The margins of the Red Sea are forming steep fault scarps, that rise sharply from the coast. In the central and southern Red Sea, the rifting area is characterized in the median valley with an axial trough that reaches water depths of more than 2000 m, and by a basaltic oceanic crust with magnetic anomalies [14]. Most of the earthquakes occur within the spreading zone in the rift valley region, which is characterized by continuous seafloor spreading [13], see Figure 1. Earthquake activities are oriented along major faults or clustered in certain spots [14]. Concentrations of earthquake activity are seen where the spreading zone is intersected by the NE-SW striking transform faults [15,16]. A great part of the seismicity of in western Saudi Arabia is volcanic-related and, thus, more of the swarm type.

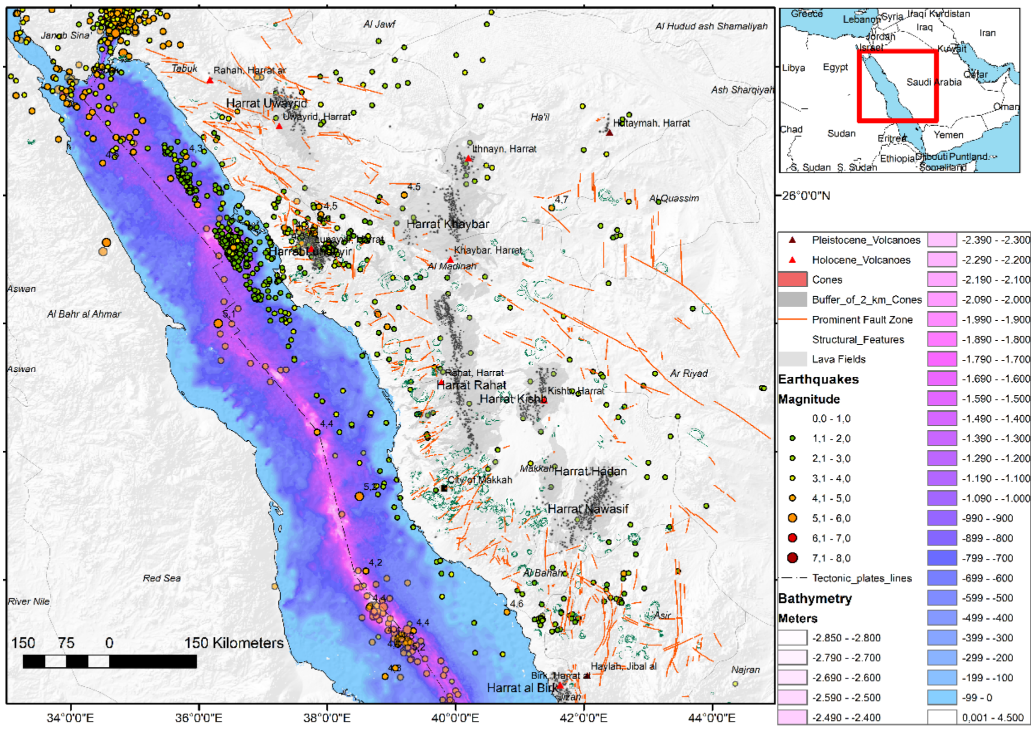

Figure 1. Earthquakes in West-Saudi Arabia (Earthquake data: USGS, ISC, EMSC) [17–19] during the last decades (sources: Lava shapefile from USGS, Pleistocene and Holocene volcano shapefiles from Smithsonian Institution's Global Volcanism Program (GVP) [20], cinder cones and larger lineaments (red lines) mapped based on satellite data).

When researching seismic and aseismic activity and the geodynamic, plate tectonic related, active movements in Western Saudi Arabia, the focus is directed towards the monitoring of larger fault zones, especially active fault zones and active shear zones. Understanding active tectonic processes have become fundamental not only for the detection of areas prone to earthquakes, but also for the monitoring of infrastructure (bridges, tunnels and pipelines).

2.3. Volcanic Hazards

The western Arabian plate encompasses at least 15 continental, intraplate volcanic fields, known in Arabic as Harrat (Figure 1). The first period of volcanism (30–15 Ma) was associated with the doming and rifting of the Proterozoic basement of the present Arabian Nubian Shield along with the north-northwest-trending rift system leading to the opening of the Red Sea basin. The second period of volcanism (<12 Ma) is characterized by north–south trending vent system associated with the onset of a new north–south trending 900 km long crustal rift system passing through the 600 km long Makkah-Madinah volcanic line.

Individual volcanic fields can be very large, such as Harrat Ash Shams and Harrat Rahat. Harrat Al Madinah volcanic province (a part of Harrat Rahat) is an active volcanic field characterized by two historical eruptions, one in 641 AD and another in 1256 AD [21]. These volcanic fields are forming a broad zone sub-parallel to the Red Sea Rift. Hawaiian to Strombolian type eruptions created lava spatter, shield volcanos and scoria cones.

Northwestern Saudi Arabia experienced notable earthquake swarms during April–June 2009. These earthquakes took place beneath Harrat Lunayyir [22]. The maximum magnitude recorded was 5.4, and this earthquake caused minor structural damage in the town of Al-Eis about 40 km from the city of Madinah [22]. As a result of this earthquake, a northwest-trending 8 km-long surface rupture propagated across the northern part of the volcanic field. Harrat Lunayyir is one of the smallest and youngest of the extensive volcanic fields on the western Arabian Peninsula, lying ~ 60 km east of the Red Sea and covering a surface area of ~3500 km^2 [23]). Historical records of volcanic activity indicate that over 20 eruptions have occurred on the Arabian Peninsula during the past 2000 years [24], including one possible eruption in Harrat Lunayyir about 1000 years ago, recent dyke intrusions monitored in 2009 [23].

2.4. Tsunami Hazards in the Red Sea Area

The potential of magmatic and volcanic activity to move large volumes of submarine materials like lava or turbidity currents that could eventually originate water mass movements has to be taken into account in the Red Sea area. Submarine, volcanic eruptions can produce volcanic tremors, earthquakes, and sudden submarine displacement of rocks and sediments, originated either by the movement of magma masses under the sea-surface, formation of fractures, effusion of lava flows, or sudden formation of islands. The capacity of submarine seismic activity (earthquakes) to produce tsunamis in the Red Sea is documented [25]. Figure 2 shows known tsunami events in the western part of the Arabian Peninsula.

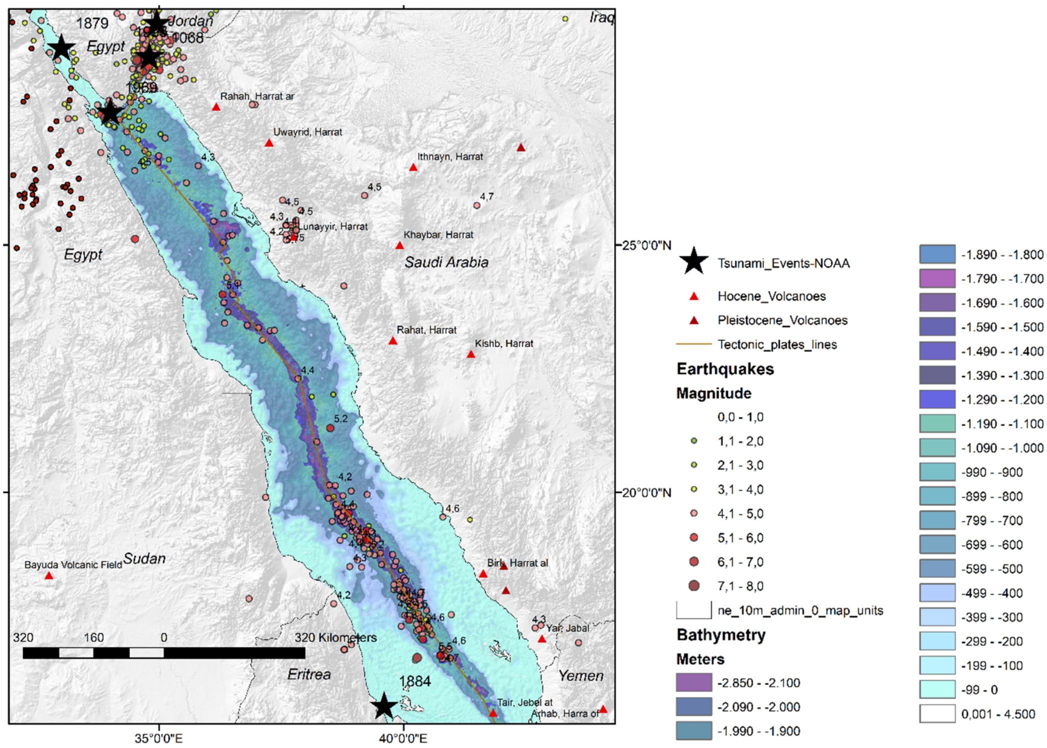

Figure 2. Tsunami events (blue stars) in the Red Sea as documented by National Oceanic and Atmospheric Administration (NOAA) [26]. Bathymetric data: General Bathymetric Chart of the Oceans (GEBCO) [27].

With an elongated shape (width of up to 355 km and a length of 2250 km) the prerequisite for seiche development in the Red Sea is given. Seiches are typically caused when strong winds and rapid changes in atmospheric pressure push water from one side of the Red Sea to the other. When the wind stops, the water rebounds to the other side of the enclosed area [28]. The water then can continue to oscillate back and forth for hours or even days. Winds and atmospheric pressure can contribute to the formation of both, seiches and meteo-tsunamis; however, winds are typically more important to a seiche motion, while pressure often plays a substantial role in meteo-tsunami formation [28].

3. Goals of this Study

Case studies for the assessment of natural hazards supported by remote sensing a GIS-tools have been carried out worldwide and in Saudi Arabia [8]. However, so far, most of the case studies are related to single, extreme geohazard events, such as volcanic eruptions or flash floods [1,29–31]. The cases that were studied have shown the value of remote sensing and GIS as a contribution to a systematic build-up of a natural hazard database according to standardized approaches in Saudi Arabia, including all kinds of geohazards and potential cascading effects.

Thus, this study is aiming to contribute to:

(a) The detection of areas susceptible to the different natural hazards, due to their specific properties and local settings.

(b) The demonstration of adapted, standardized remote sensing and GIS tools for a regularly, continuously monitoring, allowing not only the documentation of single hazard events in Saudi Arabia, but also of seasonal changes and long-term developments, such as climate change. Operational working, earth observation satellites, such as Landsat, Sentinel 1 and 2 provide the necessary, regularly updated database free of charge. Commercial satellites as RapidEye (5 m spatial resolution) and PlanetScope (3 m spatial resolution) with high temporal coverage, in case of emergency available in only up to several hours, can be used for damage assessment in short time after a geohazard. An inventory of past geohazards is one of the main prerequisites for an objective hazard assessment, which includes both the spatial and the temporal aspects of the probability of natural hazard occurrence. Such an objective hazard assessment requires a multi-source, systematic record, including regular documentation of temporal information on an occurrence that cannot be derived from a historical inventory alone. The ability to undertake the assessment, monitoring and modeling can be improved to a considerable extent through the current advances in remote sensing and GIS technology.

(c) How these tools could serve as input into a standardized natural hazard database is demonstrated in the scope of this study by the following examples:

- Flash floods: Detection of areas prone to flash flood inundation, due to their geomorphologic disposition and monitoring of areas after flash flood events;
- Seismic hazards: Mapping of fault and fracture zones and of structural features (that might be of influence on seismic hazards) based on remote sensing data;
- Volcanism: Regular inventory of volcanic features and fault zones related to volcanic activity and change detection;
- Flooding hazards in coastal areas: Detection of areas prone to tsunami flooding, meteo-tsunamis, seiche waves and storm surge. Merging the knowledge of areas prone to natural hazard with infrastructural and socio-economic data and population information provides important input for mitigation measurements and disaster preparedness.

4. Materials and Methods

The interdisciplinary approach used in the scope of this study comprises remote sensing data, climate data, geological, geophysical and geomorphological/topographic data and GIS methods (Figure 3). GeoInformation Systems (GIS), used together with remote sensing data and field research, contribute to the analysis and presentation of information related to the geohazards in the investigation area, providing input for a systematic, standardized and continuously monitoring. The processing and analysis of Landsat and Aster images of Western Saudi Arabia that have been available for decades, will support the detection of geohazards and of environmental changes, due to population growth and its related land use impact, and climate change. Different satellite data and image processing tools were tested in order to find out how far the satellite data can provide information related to the detection of causal factors influencing the susceptibility of Western Saudi Arabia to natural hazards, due to the geomorphologic and geologic disposition of the region, such as to flash floods (Figure 3).

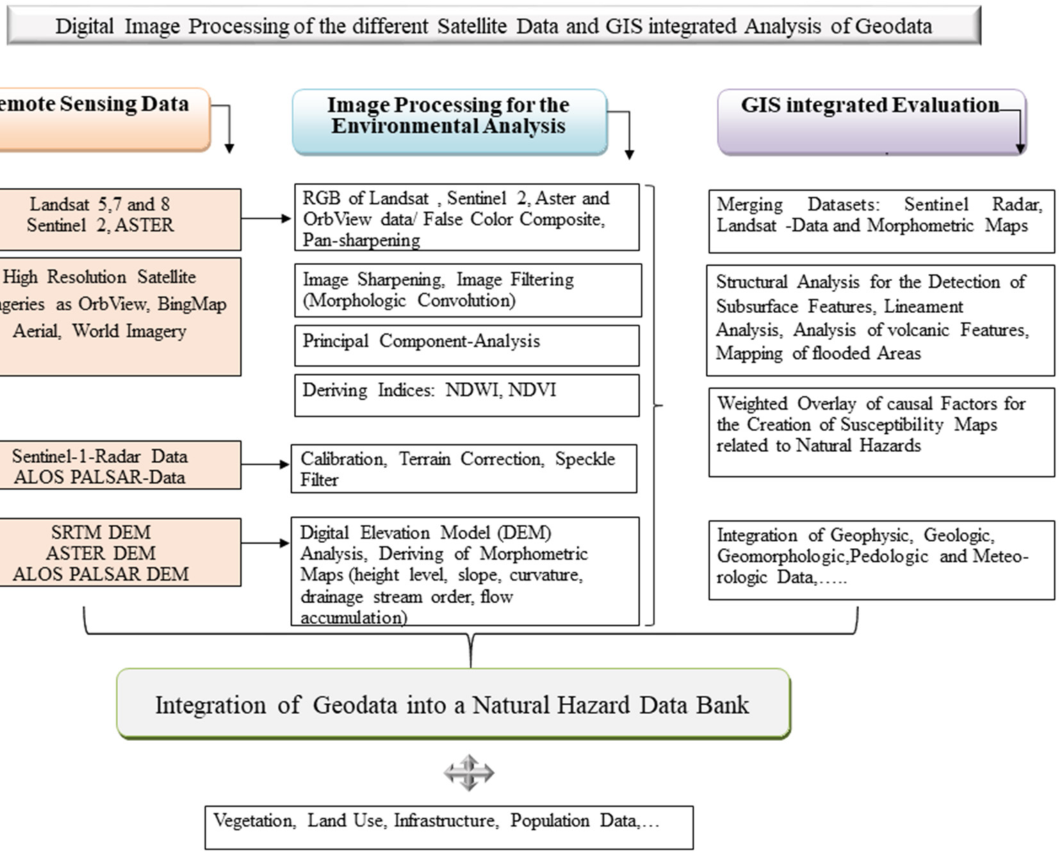

Figure 3. The workflow of data processing in Architecture Geographic Information system (ArcGIS), Sentinel Application Platform (SNAP) and Environment for Visualizing Images (ENVI) software.

The satellite data were digitally processed using image processing (ENVI, SNAP) and ArcGIS software. Based on Landsat satellite data, different false color composites (Red, Green, Blue—RGB combinations) of the different bands were used and pan-sharpened with Band 8. The chosen image processing and RGB-combinations were focused on the enhancement of geologic, tectonic and surface water information. Low pass and high pass filters and directional variations supported the detection of subtle surface structures, such as linear escarpments and ring structures. Principal component analysis (PC) of the RGB images revealed structural and lithologic information as well.

Special attention was directed at the precise mapping of traces of the tectonic pattern visible on satellite imageries, predominantly in areas with distinct expressed linear features (tonal linear anomalies, geomorphologic linear features, etc.). As the methodology of lineament analysis is an important component of this work, a short introduction into the background information is given: The term lineament is a neutral term for all linear, rectilinear or curvi-linear elements. Lineaments are often expressed as scarps, linear valleys, narrow depressions, linear zones of abundant watering, drainage network, linear vegetation occurrence, and geologic anomalies. Tonal linear anomalies, such as the linear arrangement of pixels depicting the same color /gray tone were visually mapped as linear features/lineaments as well. Lineament analysis can contribute to the detection of structural features that in the field are sometimes not visible or can be mapped only based on time and cost-intensive field investigations. As traces of structural features were digitized visible deformations, due to stress such as synclines or anticlines, bedding structures or traces of foliation in metamorphic rocks, that often appear on satellite images as dense, arc-shaped, parallel lines. Lineaments represent, in many cases, the surface expression of faults, fractures or lithologic discontinuities.

In the scope of this study, three types of linear and curvi-linear features were mapped:

- Lineaments (as a neutral term for linear features without knowing precisely their origin);
- Probable fault zones; and
- Structural features.

The mapped lineaments were compared with available tectonic data/maps from the Saudi Geological Survey [8].

One of the first steps towards the assessment of the different geohazards is susceptibility analysis and mapping. The interactions and dependencies between different causal and preparatory factors influencing the susceptibility to natural hazards can be visualized and weighted step by step in a GIS environment [32,33]. The susceptibility analysis and maps comprise the potential location of the most affected areas. Such susceptibility maps are a valuable tool for assessing current and potential risks that can be used as input for developing early warning systems and mitigation plans, such as selecting the most suitable locations for construction of structures and roads. According to the resulting susceptibility maps, hot spots can be identified where a more detailed analysis should follow. These investigations have to be combined with detailed information on historical records of both occurrences and event data are necessary for the hazard analysis.

The use of multi-temporal satellite remote sensing data opens up the opportunity for the development of efficient methods for systematic spatio-temporal mapping over large areas. For the present study, optical data as Landsat-, ASTER, Sentinel-2 and OrbView images are freely available [33]. For example, the Landsat satellites cover the same area every 16 days, the two Sentinel 2 satellites allow the coverage of the same area every five days [34].

For a better overview of seasonal influences on natural hazards, a multi-temporal analysis of different satellite data from Western Saudi Arabia should be a standard procedure. The comparative and aggregating analysis of different satellite data was carried out in this study as well in order to gain additional knowledge about the complex, geologic structure in Western Saudi Arabia, including a comparative analysis of optical satellite data (Landsat, Aster, Sentinel 2) and the Sentinel 1 and ALOS PALSAR radar data provided by the European Space Agency and the Alaska Satellite Facility [35]. The focus of the radar evaluation was directed on structural geologic information, on sediment properties related to different surface roughness and on surface water mapping.

Due to the geomorphologic situation causing distortion of the radar signals, the evaluation of Sentinel 1 A and B provided by ESA and PALSAR radar images requires geometric correction and calibration. Radar related layover-effects and foreshortening effects are limiting factors in this partly mountainous environment. The processing of the radar data was carried out using the Sentinel Application Platform - SNAP software of ESA.

The satellite imageries and DEM data were used for generating an image-based GIS database and combined with different geodata and other thematic maps of Western Saudi Arabia. This database comprises two main parts: (a) The datasets with the background geographic conditions and (b) the hazard inventory dataset. The integration of seismic records, geomorphologic analysis, digital elevation data, lithology, land cover and suitable high-resolution remote sensing data are part of this data mining. In the scope of this study, open-source data as provided by OpenStreetMap [36] or Google Earth were used in addition for gaining the necessary information, as well as evaluations of Environmental Systems Research Institute - ESRI delivered base maps and further ArcGIS-Online-tools and data.

5. Evaluation Results

5.1. Combined Evaluations of Optical Satellite Images and Satellite Radar Data for the Detection of Areas Prone to Flash Floods

Satellite images can contribute to the detection of areas prone to flash floods when acquired during or shortly after the flash flood events in Western Saudi Arabia. However, cloud covers are often a hindrance. Therefore, radar data are a valuable, additional tool for identifying flooded areas as they can be identified very clearly due to the mirror-like reflection of radar signals (black appearance on radar images). They help not only to detect areas affected by flooding, but also to visualize the related sediment flow and disposition. The monitoring and mapping of flash flood sediments and erosion pattern is an important issue for the planning of settlements, infrastructure and supply lines. Figure 4 shows a Sentinel 2 (RGB band combination of Band 8, 4 and 2) and a Sentinel 1-radar scene from an area west of the city of Mecca. Traces of sediment transport of flash floods can be easily detected on the optical satellite data of Sentinel 2 in blue colors.

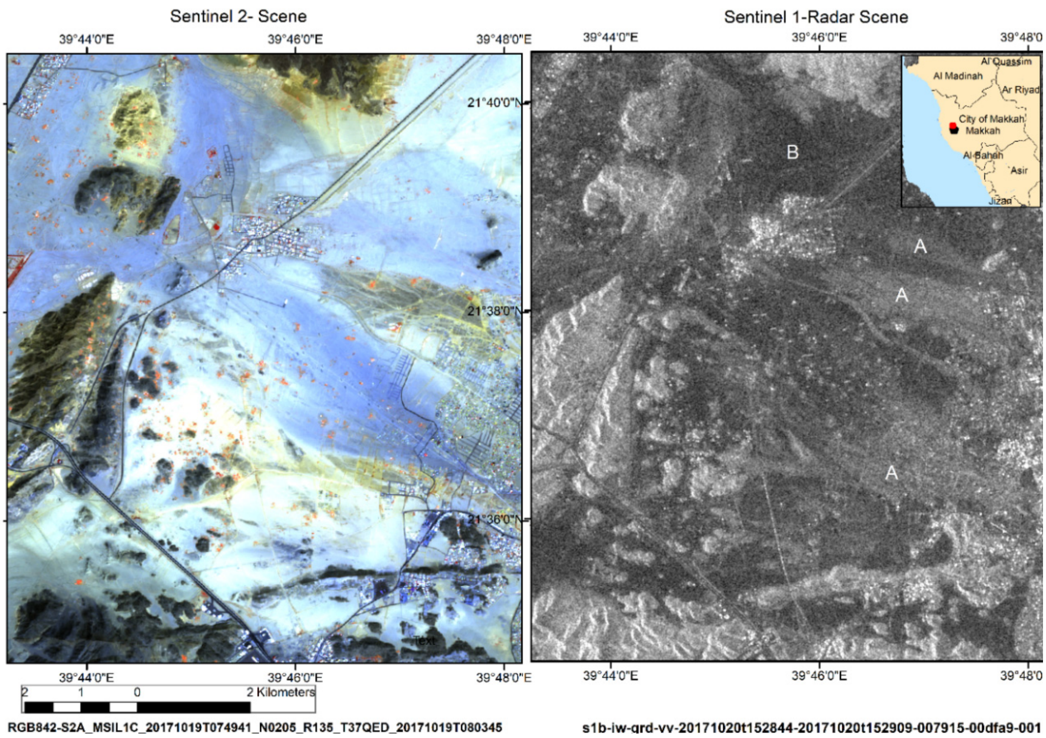

Figure 4. Sediment (blue colors) after heavy rains visible on a Sentinel 2-scene (acquisition date: 19.10.2017) and on the Sentinel 1 radar scene (acquisition date: 20.10.2017) west of the City of Mecca, (**A**)—coarser-grained sediments, (**B**)—finer grained sediments.

The differences in brightness between pixels in the radar image, marked by changes in the grayscale and backscatter intensity due to surface roughness changes contribute to the detection of sediment properties. Dark image tones are associated with finer grained sediment sheets (clay, sand) because the incident radar signals were largely reflected from their "radar-smooth" surfaces in a mirror-like fashion away from the satellite antenna. Coarse-grained sediments appear in lighter tones as their more radar-rough surfaces generate a diffuse and stronger signal return/radar backscatter (Figure 4A). As the distance to the source areas of the transported sediments during a flash flood is relatively short in this area, coarse-grained, loose gravel seems to be prevailing, thus, causing the brighter tones on the radar image (diffuse radar backscatter). The finer grained material is transported to the larger valley towards the coastal area (Figure 4B), where it is affected by aeolian activity forming dune fields.

The detailed mapping of flooded areas after flash flood events and the evaluation of the flash flood sediment properties based on radar data is suited as a standardized procedure. In this area with nearly no vegetation cover forming a hindrance against sediment transport, it is very important for damage mitigation in settlements and agricultural sites to know, where mud and debris flow is most likely to occur after flash floods. Therefore, this detailed debris flow surveillance and mapping should be part of a continuously updated monitoring in a natural hazard database.

5.2. Evaluation of Digital Elevation Model (DEM) Data

As flash floods in this area are characterized by a short duration, it is often difficult to get satellite images exactly during this time period for monitoring. In order to support the preparedness to inundations, DEM data can be used to create maps indicating those areas prone to flash floods, due to their morphometric properties. A weighted overlay procedure can be carried out for the detection of areas with higher susceptibility to flash floods by extracting causal/preparatory factors and, then, by aggregating these factors in the weighted overlay-tool of ArcGIS [32,33]. The susceptibility model represents a methodological approach to facilitate the spatial identification of flood zones. This approach is used to get information on areas that are susceptible to flash floods, due to their morphometric disposition. Flash floods occur predominantly in basin/depression-areas showing slope angles < 5°, terrain curvature = 0, high flow accumulation and drop flow according to the drop raster calculation in ArcGIS and the lowest, local height level (Figure 5). Whenever the before mentioned, causal factors occur aggregated in an area, the susceptibility to flooding is rising. Areas with these morphometric properties are susceptible to flash floods during heavy rainfall and to higher infiltration of the surface water.

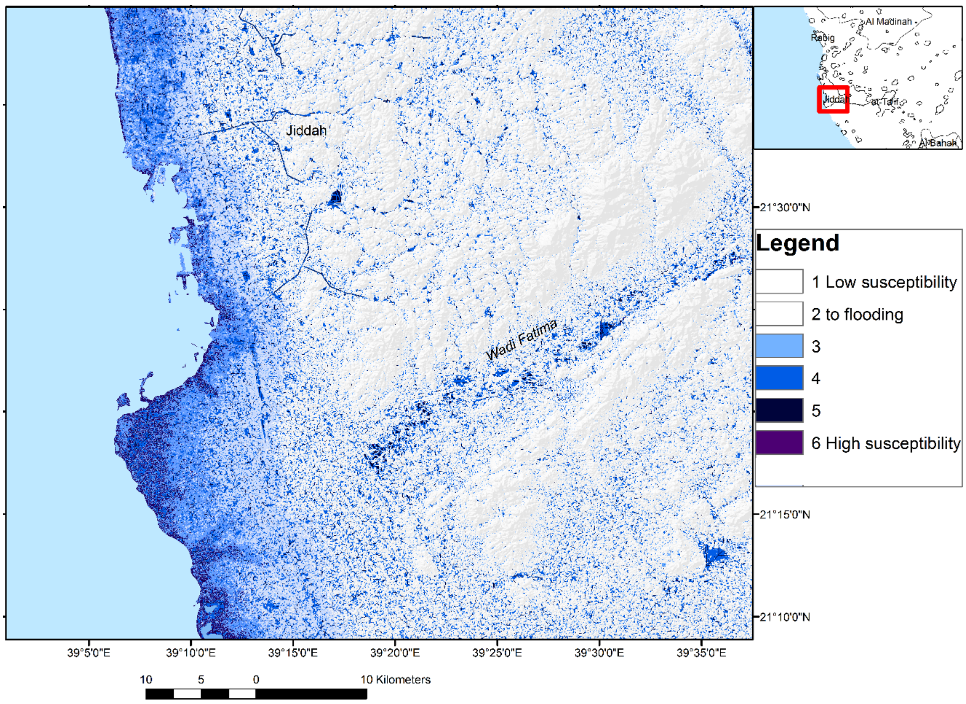

Figure 5. Weighted overlay of morphometric factors influencing the susceptibility to flooding by flash floods in the area of Jeddah showing in dark-blue the most endangered areas (factors: Curvature = 0, slope degree < 10°, height level < 10 m, dropraster calculated in ArcGIS < 100.000, flow accumulation > 5000).

As the urban development has led to the expansion of the built area into those broader valleys and basins, these areas will be exposed to flash floods after heavy rains. The knowledge of those areas that are susceptible to be flooded (the lowest and flattest areas) in those cases will help to mitigate damages, for example, by closing roads for traffic in time. As the DEM data are freely available, as well as the GIS software (QGIS), every community could prepare such a map with a spatial resolution of up to 12.5 m (provided an adapted training of the staff) to create such a database.

5.3. Structural, Tectonic Analysis of Satellite Images as Contribution to Seismic Research

The GIS integrated, structural evaluation of remote sensing data contributes to the detection of (a) larger, prominent fault zones, of (b) traces of structural features, such as ring structures or folds and (c) of traces of compression at the border zones of the Red Sea, due to the rifting processes. As the geotectonic processes and movements are dynamic processes, a continuously, comparative monitoring of the tectonic pattern using time series of satellite images is necessary.

(a) The structural/geologic evaluation of optical satellite images and of radar data allows a quite precise mapping of larger fault zones. Existing fault zones not only play an important role in ongoing tectonic processes, but also for uprising magma. They form zones of weakness that can form an entrance for the intrusion of magmatic bodies. Especially earthquake swarms were related in the past to magmatic activity [22]. The different satellite images are used, especially to detect traces of neotectonic movements in the youngest outcrops of rocks and sediments. Whereas the oldest Precambrian/Cambrian rocks show evidence of many stress imprints in the scope of earth geologic history, the youngest strata provide hints of the more actual geodynamic processes. Therefore, the Quaternary sediments and volcanic strata were investigated as well, whether traces of younger faults can be detected. Whenever distinct linear traces of fault zones and shear zones (such as scarps and valleys cutting through older lithologic units) are visible on the satellite images, there is a hint related to active faults. The principal component analysis (PCA) of Landsat data helps to identify larger, prominent fault zones and contributes to better visualization of the tectonic pattern in this area (Figure 6).

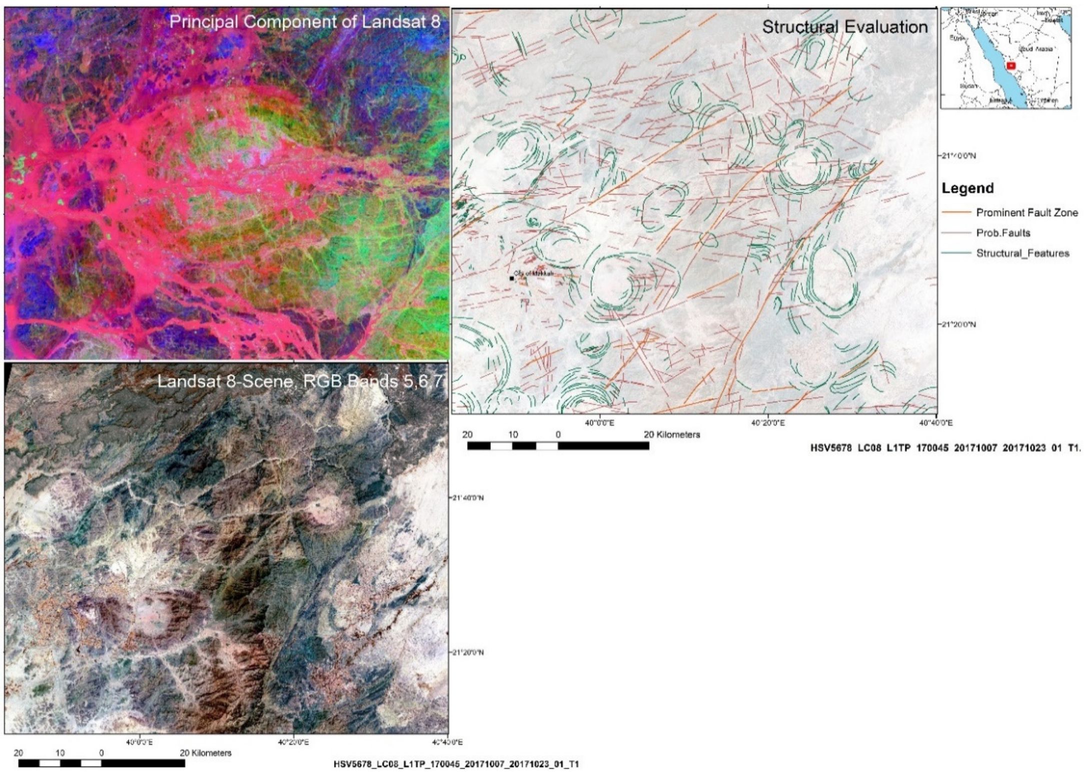

Figure 6. Image processing and structural evaluation for the detection of prominent fault zones and circular features visible on pan-sharpened Landsat 8 scenes (RGB, Bands 5,6,7 and 8 and derived PC, acquisition date: 07.10.2017).

(b) Another important aspect is the detection of circular structures in the Precambrian and Cambrian rocks, even when deeply eroded and only visible on the satellite images because of the circular outline. The annular structures show circular or oval shapes, and they are different, in their structures, from other surrounding geologic phenomena, most of them consisting of intrusive batholiths [37]. These ring-shaped structures differ in their dimensions, origin and the characteristics of their identification on satellite images. Some form prominent domes; others are only visible, due to circular, tonal anomalies in the sedimentary covers. Their dimensions range from many meters till hundreds of meters up to more than 100 km. The majority of these circular structures with 10 to 25 km in diameter were generally created by Precambrian intrusive, magmatic bodies of different mineralogical composition (mainly granitic) and geomechanic properties.

The knowledge of the position of circular structures plays an important role when dealing with seismic and aseismic movements in this area. The earthquake pattern might be influenced by the circular structures, as well as the recent volcanic activity. It seems as if the larger fault zones are "bending" around the structures. The structural analysis is presented in Figure 6, based on visual evaluations. An automatic lineament extraction would provide results with errors, due to numerous roads in this area or sedimentary covers over outcropping rocks.

For a better understanding of the geomechanic processes in this area (movements towards the northeast with velocities of 10 to 15 mm/year [38], it has to be considered that the intrusive bodies might react mechanically different than the surrounding rocks, potentially forming asperities that could lead to earthquakes in case of stress accumulation. Ring structures with their different, geomechanical properties, especially when occurring block-wise, form a relatively stable "hindrance" against tectonic movements and magmatic activity. Therefore, their precise, structural mapping, including the tools of remote sensing and GIS might contribute to a better understanding of the seismic activity in Western Saudi Arabia.

During the last decades, only a few earthquakes were documented within the area of the circular structures [17–19]. In the case of stronger earthquakes, even far-field ones, these circular structures could influence seismic wave propagation and would cause lateral variations in seismic wave speeds.

Especially the thermal bands of ASTER and Landsat 8 and Sentinel 1 radar images allow the detection of circular structures that often cannot be detected in the field easily, due to sedimentary covers. Due to the penetration capabilities of Sentinel 1- C-Band radar into unconsolidated sedimentary covers up to several dm subsurface structures become visible that often remain partly undetected on optical satellite images. The satellite radar images of this arid area clearly reveal penetration of the radar signals through covers of eolian and flash flood /fluvial deposits. Penetration of the masking sand covers facilitates the detection of the underlying surface, due to the reflection at the sand/bedrock interface. Dark image tones are associated with deeper sand sheets because the incident radar signals were largely reflected from their "radar-smooth" surfaces in a mirror-like fashion away from the satellite antenna (Figure 7). The granitic rocks and gneisses appear in lighter tones as their more radar-rough surfaces cause a diffuse and stronger signal return/radar backscatter. The ring structure, shown in Figure 7, appears even more detailed on the radar scene (Figure 7, image 4), due to the subtle differences in the radar reflection. Thus, satellite data help considerably to a systematic inventory of ring structures, however, not revealing their geologic origin.

Lineaments maps should be part of a natural hazard database. Web-services, such as those provided by Bhuvan, India, [5] already offer lineament layers for the users as a standard procedure.

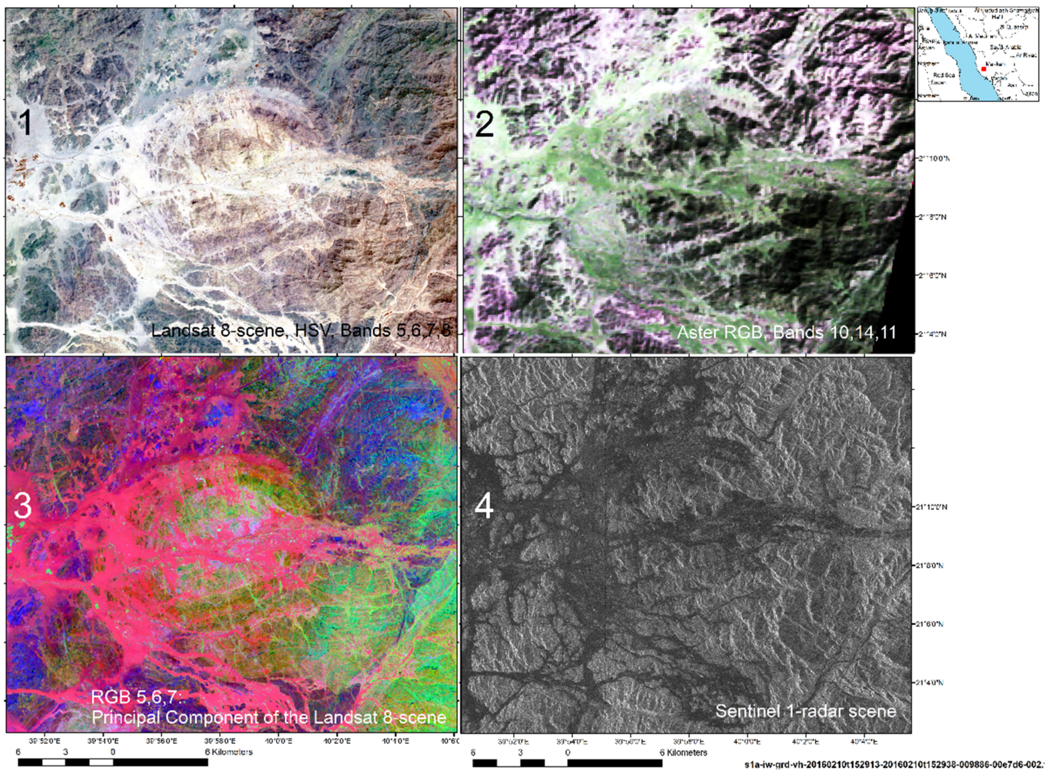

Figure 7. Use of different satellite data for providing structural information on a circular structure in the south of Makkah. (**1**)—Landsat 8, HSV, Bands 5,6,7,8 LC08_L1TP_170045_20171007_20171023_01_T1. (**2**)—ASTER, RGB, Bands 10,14,11-AST_L1T_00301032018080650_20180104121027_17567. (**3**)—Principal component (PC) of the Landsat 8-databased on the RGB of Bands 5,6,7. (**4**)—Sentinel 1-radar image, s1a-iw-grd-vh-20160210t152913-20160210t152938-009886-00e7d6-002.

(c) The coast-near areas clearly show evidence of linear features oriented NW-SE to NNW-SSE parallel to the axis of the Red Sea rift valley (Figure 8). As the area is moving towards NE, theses curvi-linear features might be related to traces of compression, due to accretionary thrusting and thrust-related structures. The striking direction of the assumed traces of compression changes in close relation, parallel to the orientation of the rifting axis from NW-SE to NNW-SSE. SW-NE oriented, linear elements, perpendicular to the rift valley main axis, are very prominent on the satellite images as well. Of course, there is a need to verify these features in the field. These linear features could be partly correlated with known larger shear zones, such as the Wadi Fatima shear zone [16]. Examples of the visibility of these traces are shown in the next figures (Figures 9–11).

Linear tonal anomalies and linear morphologic features help to detect larger fault zones on radar images. The differences in brightness between pixels in the Sentinel-1 radar image (Figure 11), marked by changes in the grayscale and backscatter intensity, due to surface roughness changes contribute to the location of fault zones. The illumination geometry of the radar signals from the west supports the detection of fault zones parallel to the rift zone.

Traces of probable compression can be visualized as well by processing of DEM data in order to enhance linear depressions and ridges oriented perpendicular to the main stress field. A digital map of depressions can be obtained by the map algebra operation of subtracting the depression-free DEM from the original DEM: (Fill-Aster-Mosaic)—(Aster-Mosaic) or the Sink-Tool in ArcGIS. The methodology is a semi-automatic approach involving several steps: (a) DEM acquisition and (b) sink-depth calculation using the difference between the raw DEM and the corresponding DEM with sinks filled.

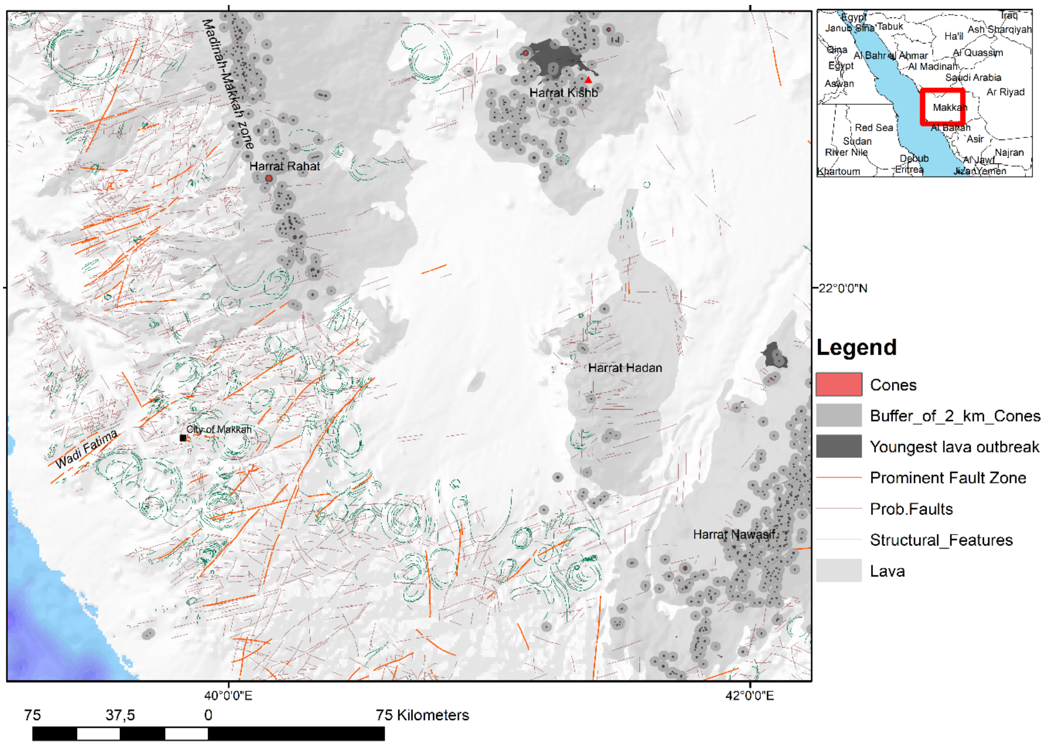

Figure 8. Larger, prominent lineaments, ring structures and volcanic features mapped based on different satellite data (Landsat, Sentinel, Aster).

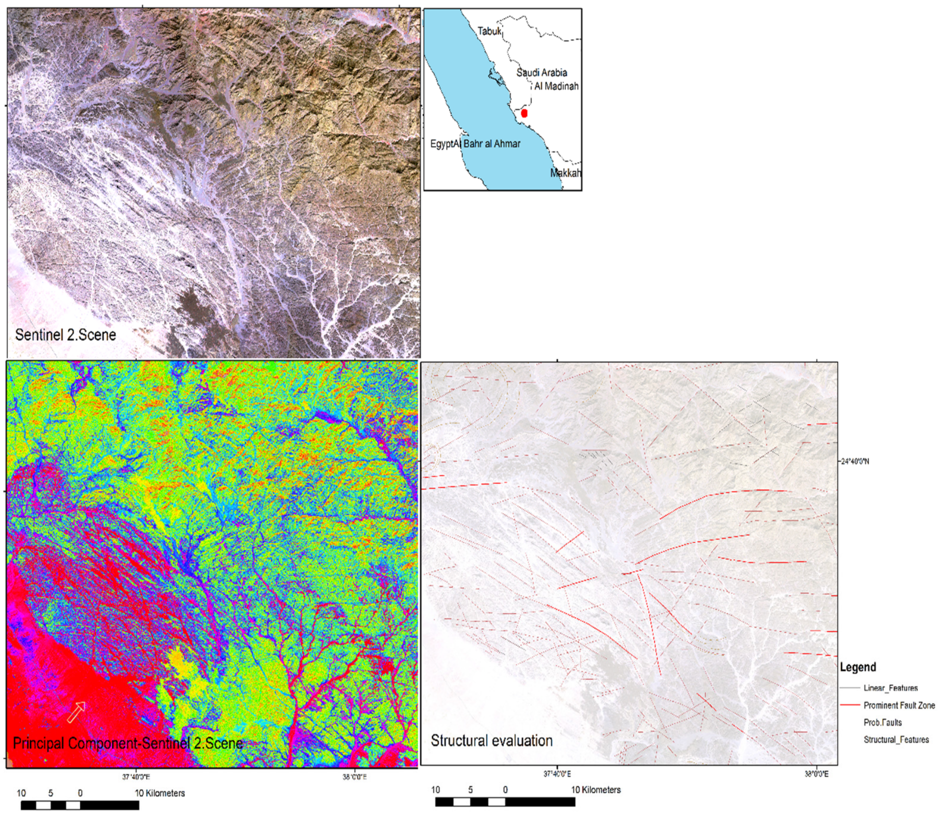

Figure 9. Traces of compression visible as parallel, NW-SE—oriented linear features perpendicular to the direction of the main stress. Visible on Sentinel 2, RGB of Bands 8,4,2, and derived PC (Acquisition date: 26.11.2018).

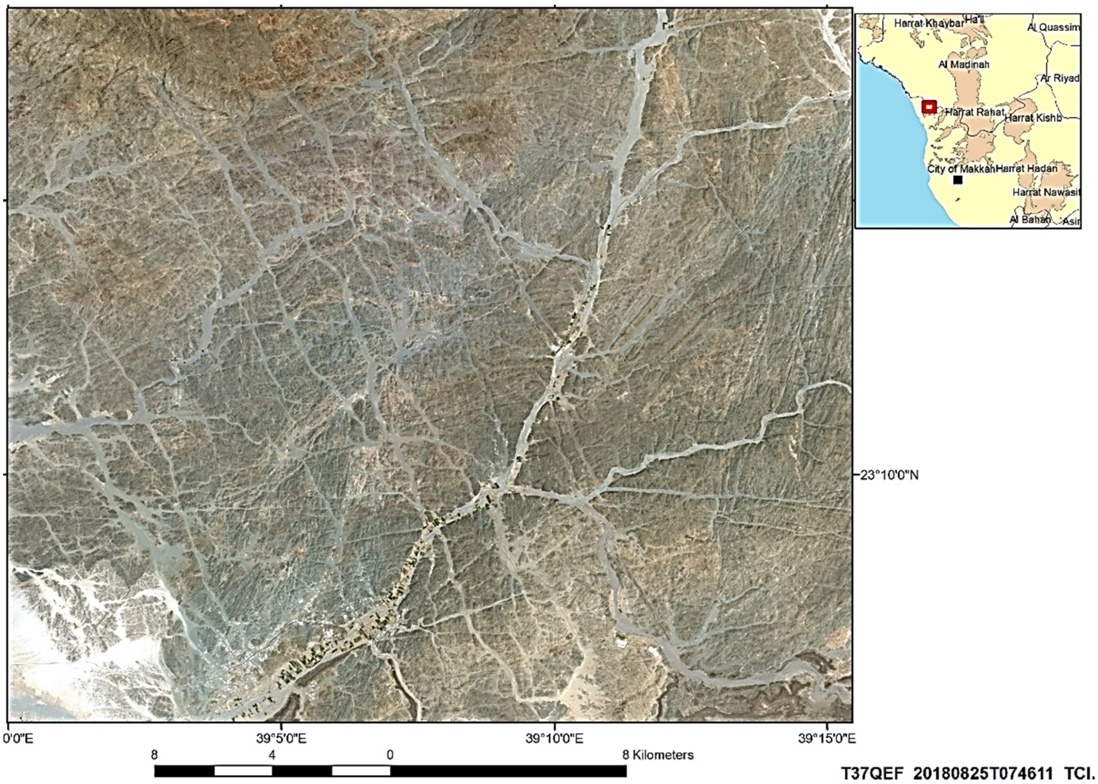

Figure 10. Traces of compression visible on a Sentinel 2 scene (RGB, Bands 4,3,2, acquisition date: 25.08.2018).

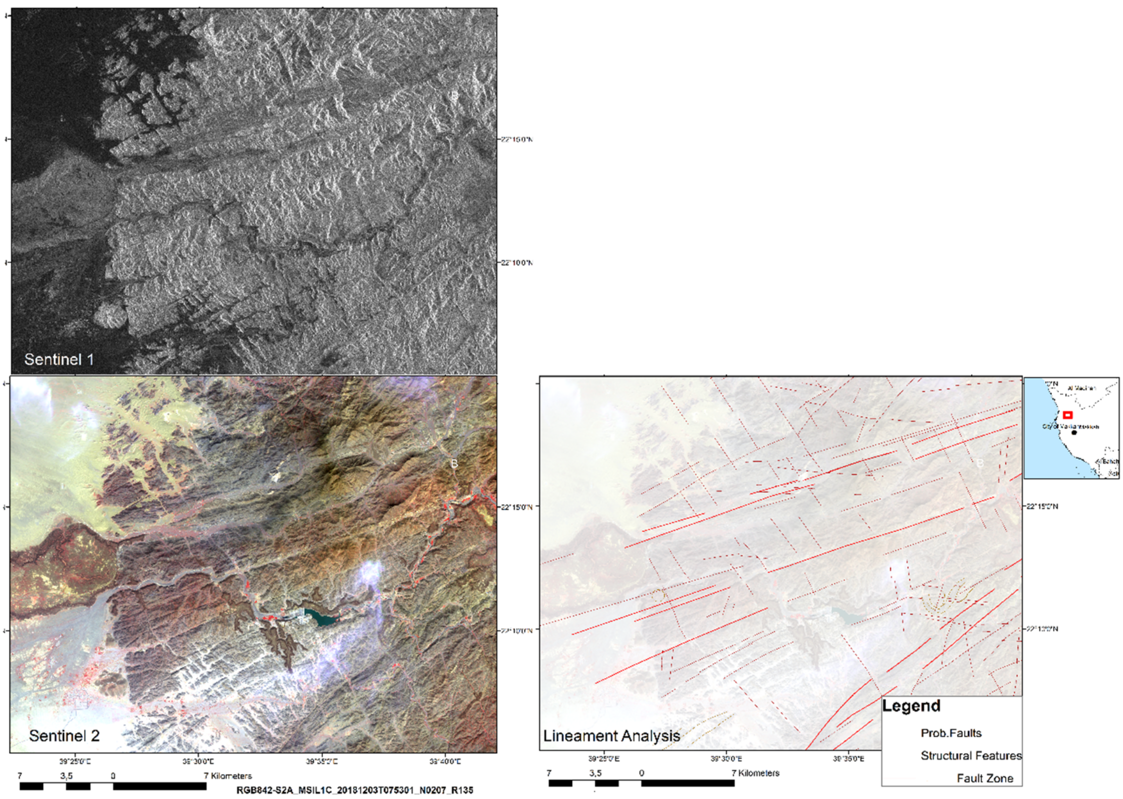

Figure 11. Traces of compression visible on Sentinel 1 radar and Sentinel 2 optical images (Sentinel 2: RGB, Bands 8,4,2) as NW-SE oriented parallel, linear features.

The first step comprises the “Fillsink” algorithm from the ArcMap software package that identifies the point or set of adjacent points surrounded by neighbors with higher elevation and rises to the lowest value on the depressions boundary. This procedure then fills all depressions in the DEM, including both those generated from data errors (spurious artifacts) and those that record real topographic features.

The second step extracts the sink depths in these areas by differencing the maps between the sink-filled (“depressionless” DEM) and original DEM. The difference image highlights the different depressions [32]. This approach was carried out based on SRTM, Aster and ALOS PALSAR DEM data, comparing the results. When evaluating the DEM difference maps of all the three DEM data sets, a linear, parallel arrangement of the sinks becomes visible, oriented parallel to the coast, even in the youngest sediments (Figures 12 and 13). The origin of this parallel, linear arrangement might be complex and has to be discussed and to be further investigated: Reasons among others might be a) compression of the subsurface, b) traces of uplift, c) traces of parallel longitudinal dunes underneath the younger eolian covers, linear wind erosion, and flash flood sediments? Due to the rifting processes in the Red Sea and the movements of the Arabian Plate towards NE with velocities of about 10 to 15 mm/year, it seems most likely that the parallel alignment of linear features is related to compression [13,38,39].

When comparing the position of earthquake epicenters with the lineament map of W-Saudi Arabia, it appears, that the earthquake epicenters occur concentrated along these SW-NE striking shear zones (Figures 1 and 2). Whether these earthquakes were triggered by stress accumulations along fault zones or by magmatic activity in the subsurface, or the combination of both, has still to be investigated more detailed in the affected areas. In the scope of this study, the monitoring of those zones of weakness is important regarding the safety of infrastructure. The relatively youngest, prominent fault zones cutting even through Holocene sediments, striking N-S, are visible on the different satellite data as linear, tonal anomalies.

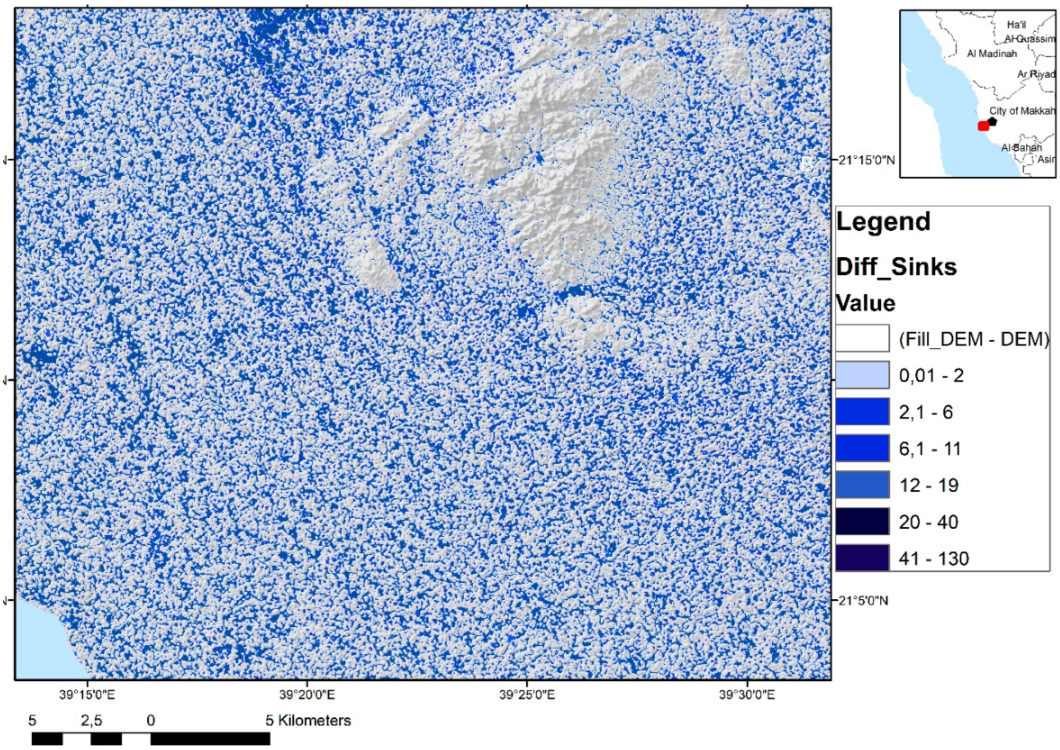

Figure 12. Difference DEM map of the coastal area of Jeddah showing a linear, NW-SE oriented, the parallel arrangement of the “sinks” in the SRTM-DEM.

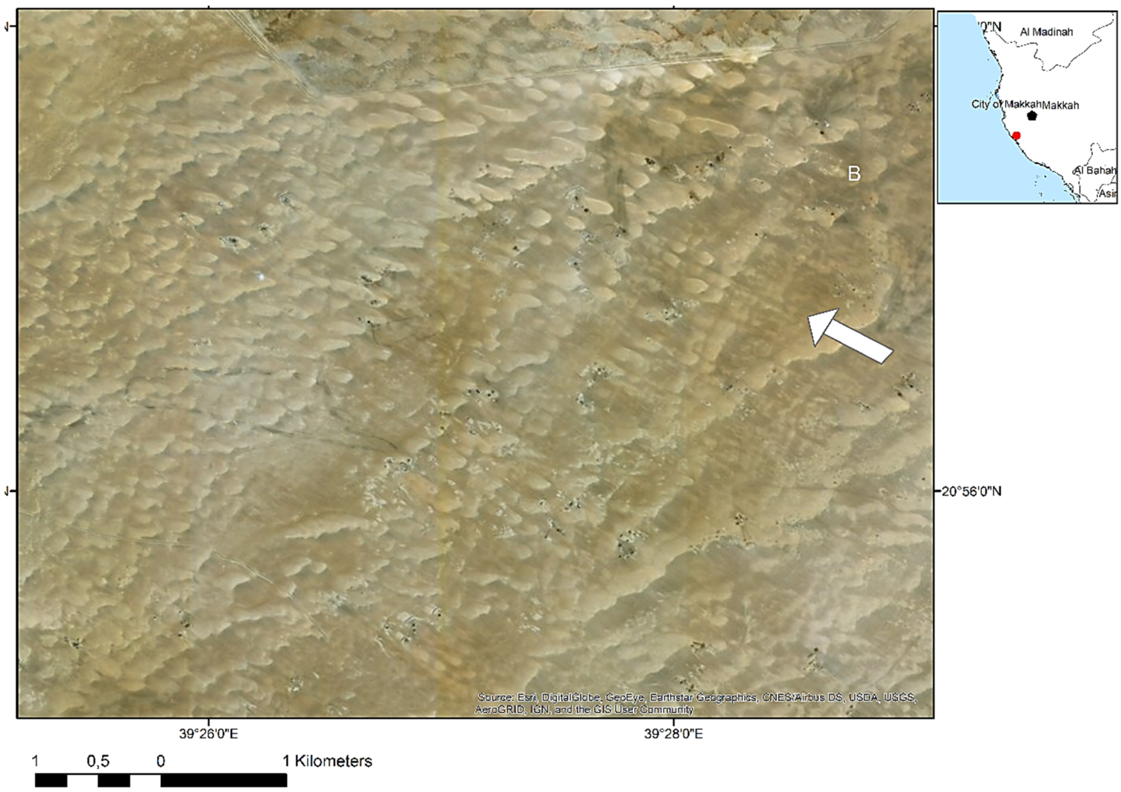

Figure 13. Parallel, linear, NW-SE oriented features within coastal dune fields visible on World Imagery-layers provided in ArcGIS by the Environmental Systems Research Institute (ESRI).

5.4. Contribution of the GIS Integrated Evaluation of Satellite Data to the Monitoring of Volcanic Features

After digital image processing of Sentinel 2, Landsat 8, ASTER and OrbView data the use of satellite data for volcanic monitoring becomes evident: Remote sensing and GIS can contribute to,

- The mapping of volcanic cinder cones;
- The mapping of visible fault zones and dikes in the area of cinder cone fields;
- The mapping of the most recent lava flow;
- The detection of traces of age differences and types of volcanic features based on erosional and weathering conditions and on the lithologic composition.

A systematic inventory and mapping of cinder cones and youngest volcanic eruptions in the different volcanic areas was carried out, combined with a structural (lineament) analysis (Figure 14).

Digital image processing tools in ENVI, SNAP and ArcGIS software help to identify cinder cones by using RGB band combinations and Gaussian filters, or a principal component analysis. About 2500 cinder cones were digitized in the adjacent areas of the Red Sea Red. The size of the cinder cones is relatively constant about 200 to more than 1000 m in diameter (Figure 15). The mapping of the relatively youngest traces of volcanic activity, such as dyke intrusions or most recent lava outbreak provides information on fault zones that are susceptible to magmatic uprise. Such information is important for the understanding, where and when future eruptions are likely to occur. This might be important for volcanic hazard preparedness. Thus, the structural evaluation of the different satellite data is used to identify those fault zones that are obviously related to magma ascent. The strike and type of those fault zones changes from north to south. Whereas in the northern part, mainly NW-SE oriented fault zones are dominant, in the central part of western Saudi Arabia NNW-SSE, and N-S striking fault zones are prevailing (Figure 7). The concentration of volcanic cones along the NNW-SSE oriented Madinah-Makkah volcanic line [40] is clearly visible. In the southern part, NE-SW oriented fault zones are influencing the volcanic pattern as in Harrat Nawasif. Special attention is directed to the intersection of larger fault zones. Whenever prominent SW-NE striking fault zones are crossing N-S-oriented ones in the Harrat areas, a concentration of cinder cones align along the fault zones in the intersections can be observed.

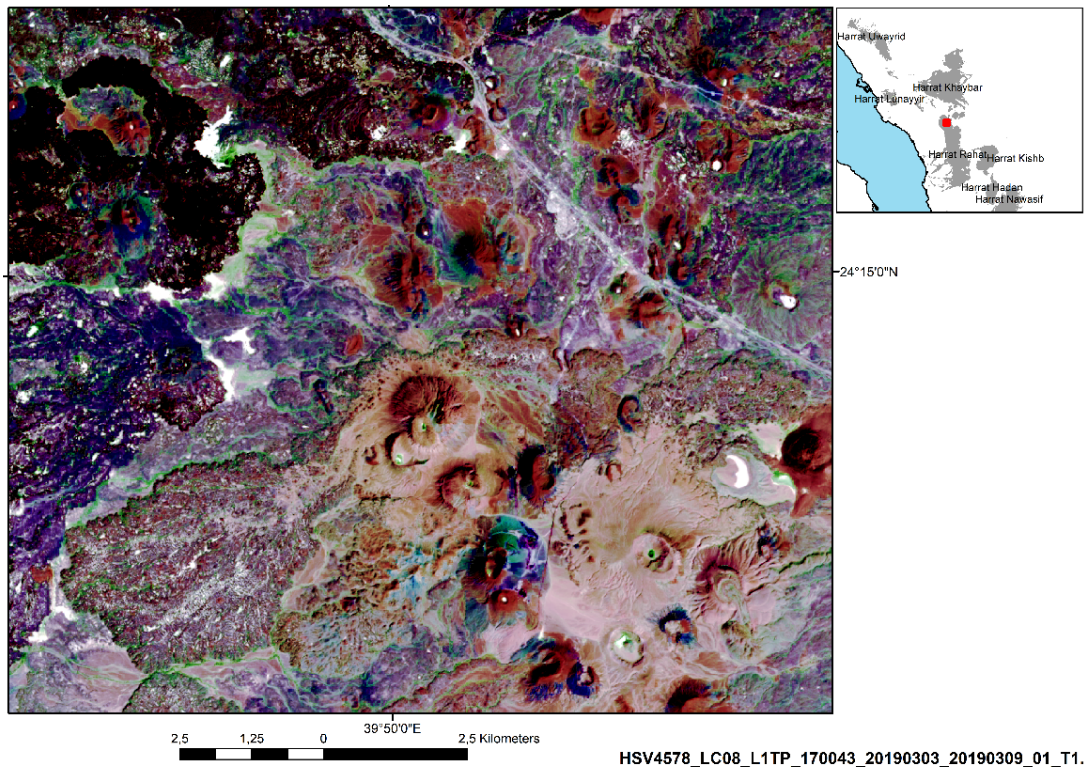

Figure 14. Cinder cones of alkali-olivine basalt (red) aligned along N-S and SW-NE oriented fault zones and recent lava outbreak areas [19] with thin fluid basalt lava flows in the north of Harrat Rahat visible on a pan-sharpened Landsat 8 scene (HSV, Bands 4,6,7,8, acquisition date: 03.03.2019).

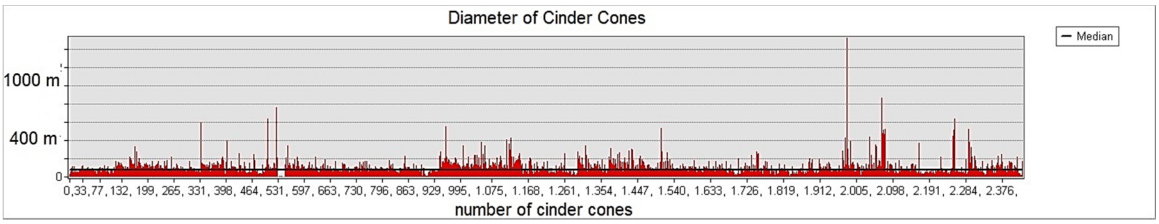

Figure 15. Size of cinder cones (based on about 2500 mapped cinder cones) in the Red Sea area.

The question arises, why the volcanic activity of Harrat Rahat has stopped in the N of the City of Mecca? The volcanic activity of the Madinah-Makkah zone (comprising the area along the NNW-SSE axis of Harrat Rahat) almost stops along the SW-NE oriented Wadi Fatima shear zone (Figure 8). Lava fields and cinder cones occur as if shifted towards the east in the area of Harrat Hadan and Harrat Nawasif. As one of the explanations for this phenomenon might be discussed the occurrence of ring structures: When analysing the position of circular structures and the outcrop of lava, it seems as if the circular structures have an influence on the occurrence and shape of the lava flow. Obviously larger, compact intrusive bodies are forming a hindrance for uprising, larger, volcanic intrusions. In areas with a higher density of large circular structures, such as in the area of Makkah younger lava sheets and cinder cones could not be observed. However, the larger ring structures are often intersected by dykes.

The following Sentinel-2 RGB-scenes (Figures 16–18) show circular features that are partly surrounded by younger lava sheets. Whether this is caused only by topographic reasons as some ring structures are forming domes causing a flowing around, or/and selective erosion or by circular structures hindering recent magmatic ascent and flow, this has still to be investigated in the specific cases.

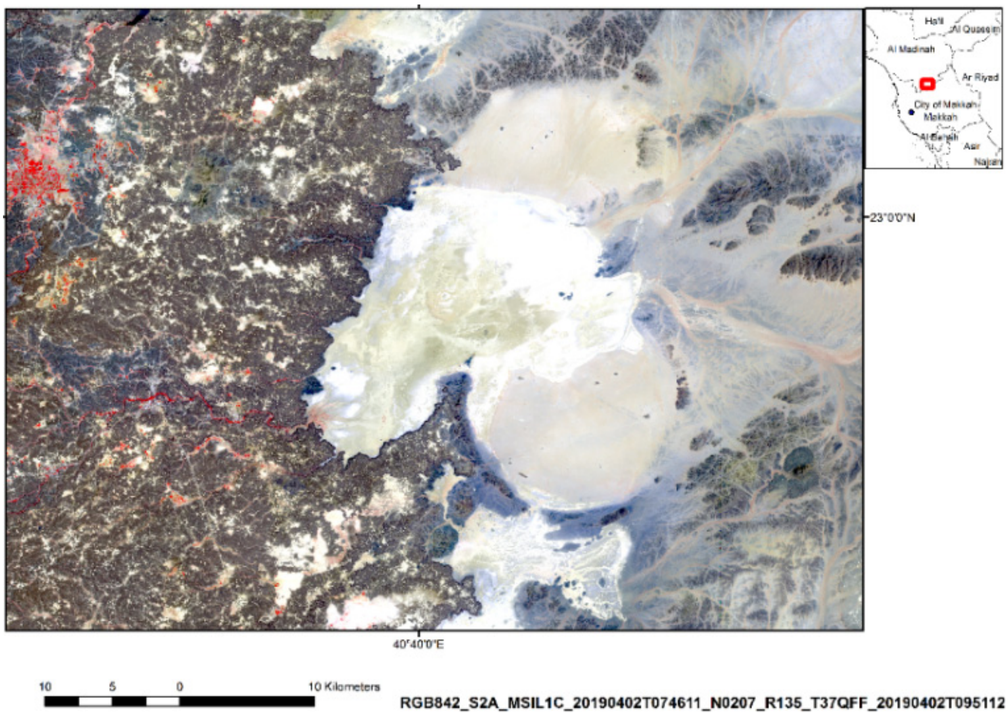

Figure 16. Sentinel 2-scene (RGB: Bands 8,4,2, acquisition date: 02.04.2019) showing ring structures in the east of Harrat Rahat surrounded by lava in the western part.

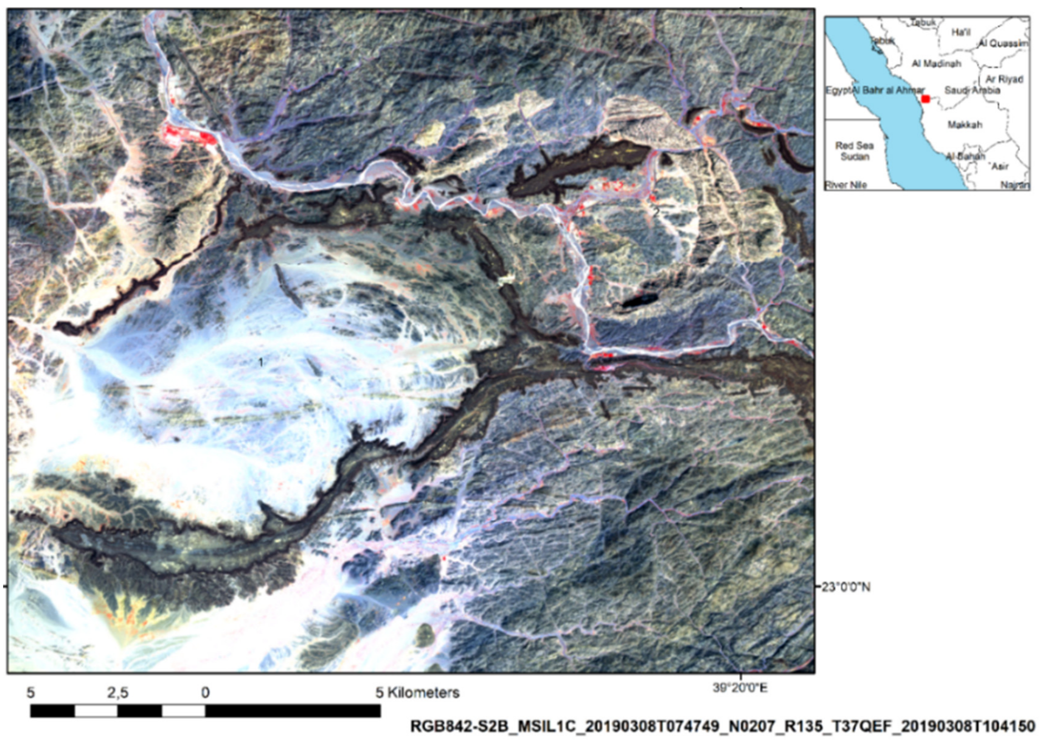

Figure 17. Lava flows around oval (left) and circular (upper right) shaped structures (Sentinel 2: RGB, Bands, 8,4,2, acquisition date: 08.03.2019).

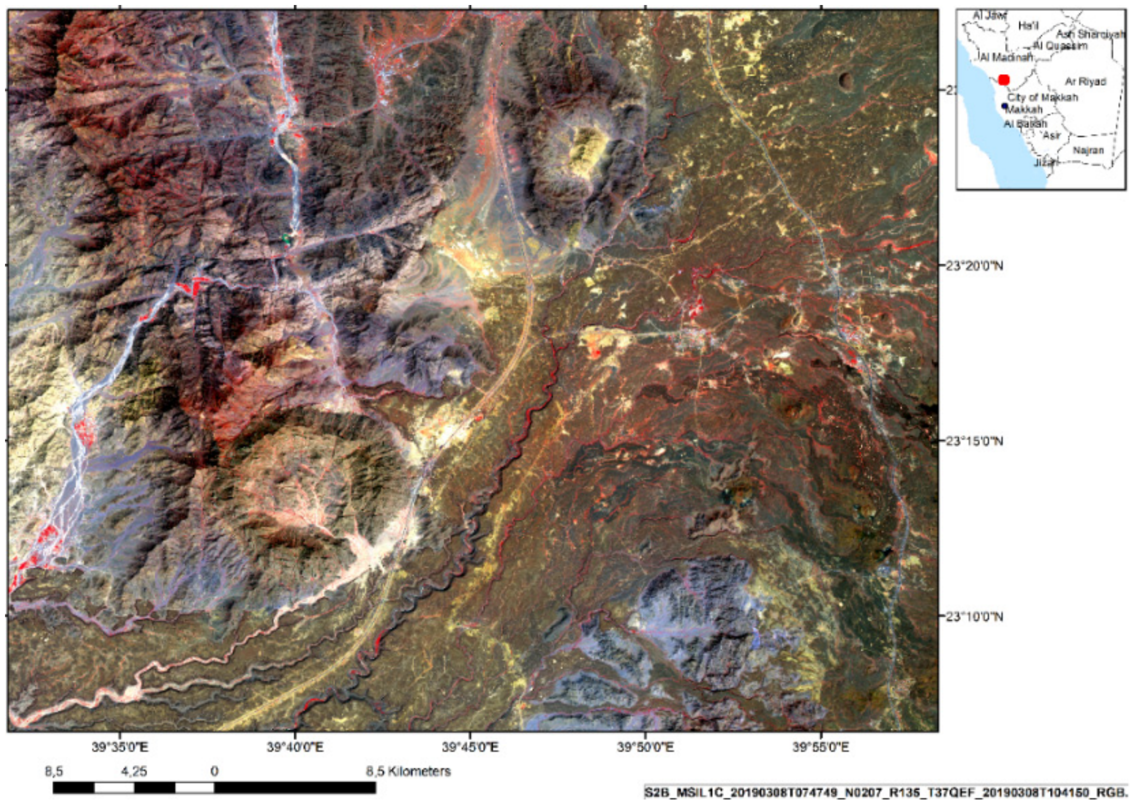

Figure 18. Lava sheets surrounding ring structures (Sentinel 2: RGB, Bands 8,4,2, acquisition date: 08.03.2019).

Based on evaluations of satellite data it is possible to categorize the different volcanic features in W-Saudi Arabia systematically based on the geomorphologic properties, erosional and weathering conditions and on the lithologic composition:

- Cinder cones with latest lava outbreak, intact lava sheets,
- dissolved and intersected lava sheets and lava inselbergs,
- lava fields with developed drainage system, and
- isolated volcanic features intersecting eolian and fluvial sediments,

Dissolved lava sheets and inselbergs occur predominantly at the western part of the Harrats, whereas the lava sheets in the eastern part are characterized by the development of a dense drainage pattern and small depressions filled with evaporitic and youngest sedimentary covers (Figures 1–4 and 19).

The regularly updated monitoring of volcanic features, of their tectonic pattern and vertical movements by combining different satellite data, seismic, geodetic and geologic data forms an important part of a natural hazard data stock. A focus of the comparative, temporal analysis of satellite data in time series should be the tracing of potential changes in volcanic areas. When integrating the monitoring results into a natural hazard database, changes of the fault pattern or new lava flow areas could be detected immediately and, then, be part of disaster risk management.

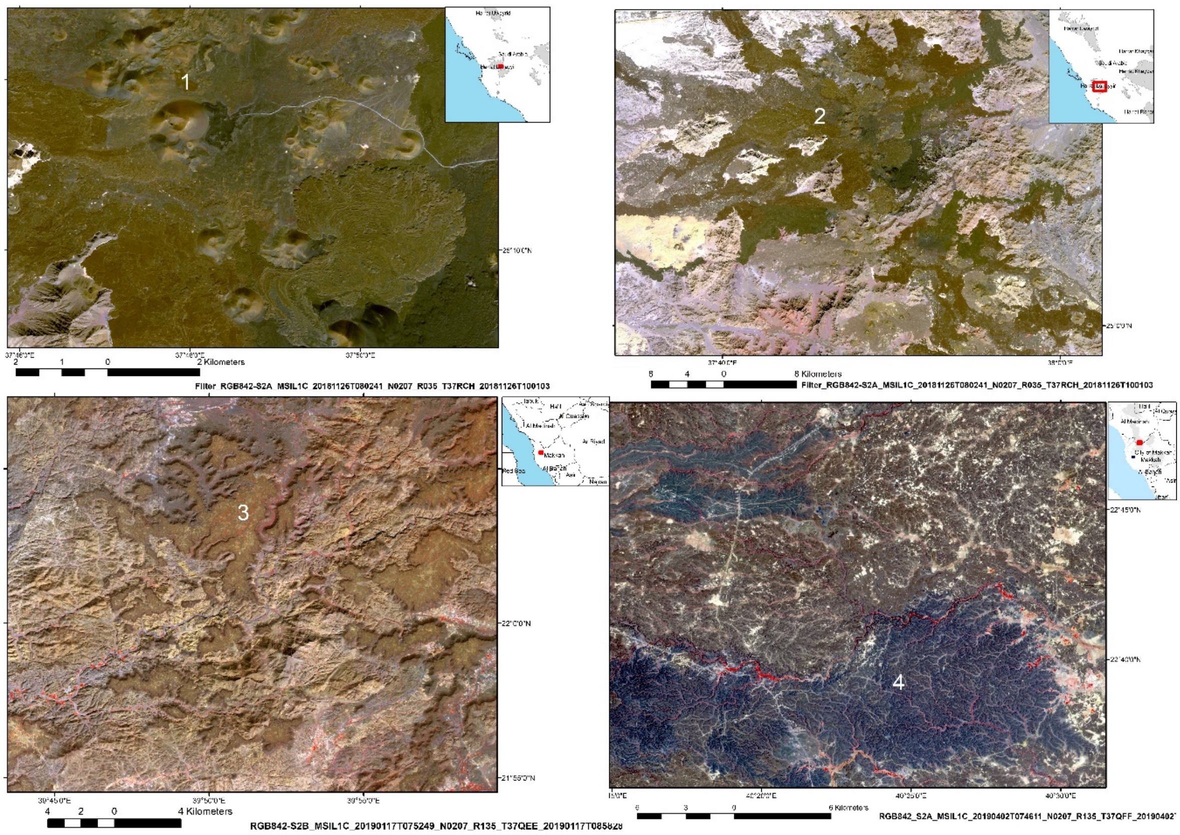

Figure 19. Geomorphologic types of volcanic features visible on Sentinel 2 scenes. (**1**)—cinder cones, (**2**)—lava outbreak with high lava viscosity, (**3**)—lava inselbergs, (**4**)—eroded lava sheets with drainage patterns.

5.5. Contribution of Remote Sensing and GIS to the Detection of Factors Influencing Tsunami Hazard

The input of remote sensing and GIS can be considered only as a small part of the whole "mosaic" of tsunami research approaches. Nevertheless, it offers a low-cost to no-cost approach, that can be used as the first basic data stock for emergency preparedness by providing, for example, susceptibility-to-flooding maps. Summarizing factors influencing flooding susceptibility, such as relatively low height levels (<10 m) help to detect areas with higher flooding susceptibility. Those areas might be prone to flooding in case of a severe tsunami event. The following Figure 20a,b show an example of the city of Jeddah, intersecting road-shapefiles with height levels below 5 m, assuming a tsunami wave-height of 5 meters as the leading parameter for tsunami preparedness. In case of high energetic flood waves from the Red Sea or in case of flash floods, these road segments < 5 m might be prone first to flooding, due to their lowest height level. For strengthening urban resilience planning such maps could be helpful by indicating those road segments that are susceptible to flooding in case of flash floods. Previous flooding events in this city in 2009 and 2011 with heavy human and material losses [41] have demonstrated the necessity of such maps.

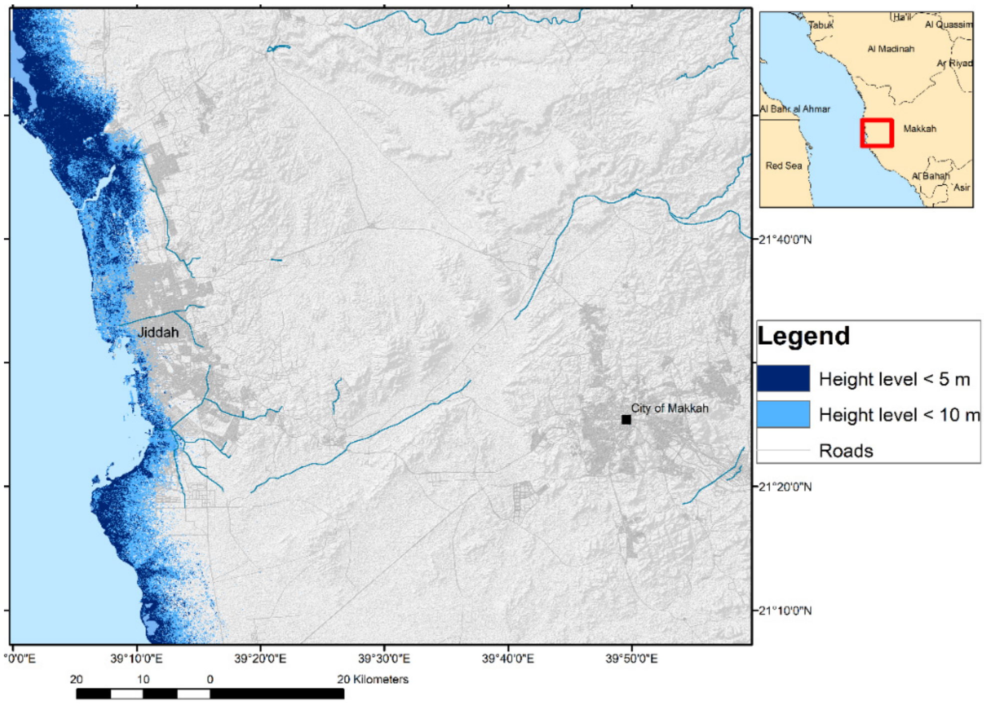

(**a**)

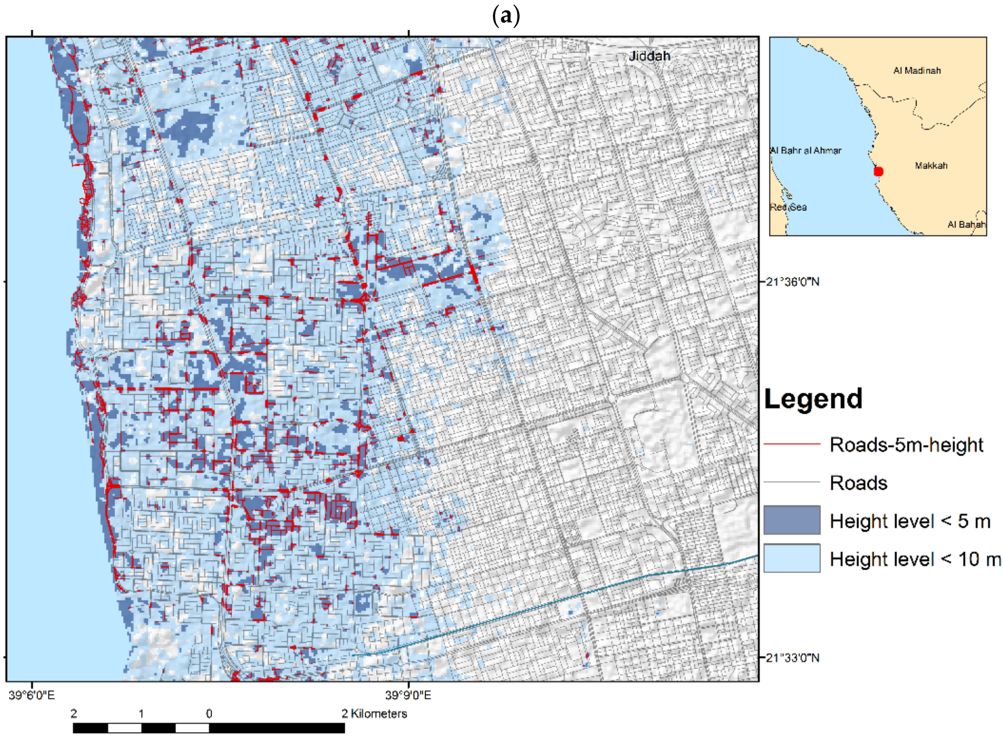

(**b**)

Figure 20. (**a**) Height levels below 10 m calculated based on SRTM DEM data (30 m resolution). (**b**). Road segments below 5 m height level (red) in Jeddah calculated based on ALOS. PALSAR DEM data (12.5 m resolution).

The source of tsunami waves, the direction of the incoming waves, and their height and energy cannot be predicted. However, when analysing the influence of the coastal morphology on the streaming pattern in relation to wind and wave directions, it supports a better understanding of what might happen in case of high energetic flood waves. Given that coastal flow is the product of a complex mix of factors (i.e., freshwater discharge, tides, temperature, salinity, winds in various frequency bands and the influence of motions imposed from seiche movements), coastal dynamics may be regarded almost as regional. The tide amplitude at the time of a potential tsunami directly affects the inundation height as well and, hence, the impact of the tsunami on the coastal areas. Even in the case of small amplitude tsunamis, the combination of the tsunami with a higher tide might result in higher wave height.

Satellite scenes reveal a streaming pattern of the upper cm of the water surface. After digital image processing and enhancement, especially of the thermal LANDSAT and ASTER bands from the coastal areas, water currents at the acquisition time become clearly visible. Of course, these images reflect the water, wind and temperature conditions at the data acquisition time. However, the streaming pattern visible on the LANDSAT imageries provides some useful information on the influence of coastal morphology on water currents, that might be of interest for the better understanding of storm surge, meteo-tsunamis and tsunami wave propagation and their interaction with the coastal morphologic properties.

Evaluations of time series of LANDSAT or Sentinel 2 imageries form an important input, as the images contribute to a better understanding of the streaming pattern among different conditions, such as wind directions and intensities, or seasonal temperature and salinity changes. The next figure (Figure 21) shows Landsat 8-senes (RGB band combination 2,1,7) of different acquisition times with different wind and streaming conditions. Islands in front of the coastline are influencing and modifying the wave patterns, their density and sizes (Figures 21 and 22), often causing turbulent flows. Depending on the wind direction waves are interfering each other within the area of the islands. The islands situated in front of the coastline might slow down high energetic flood waves directed towards the coast.

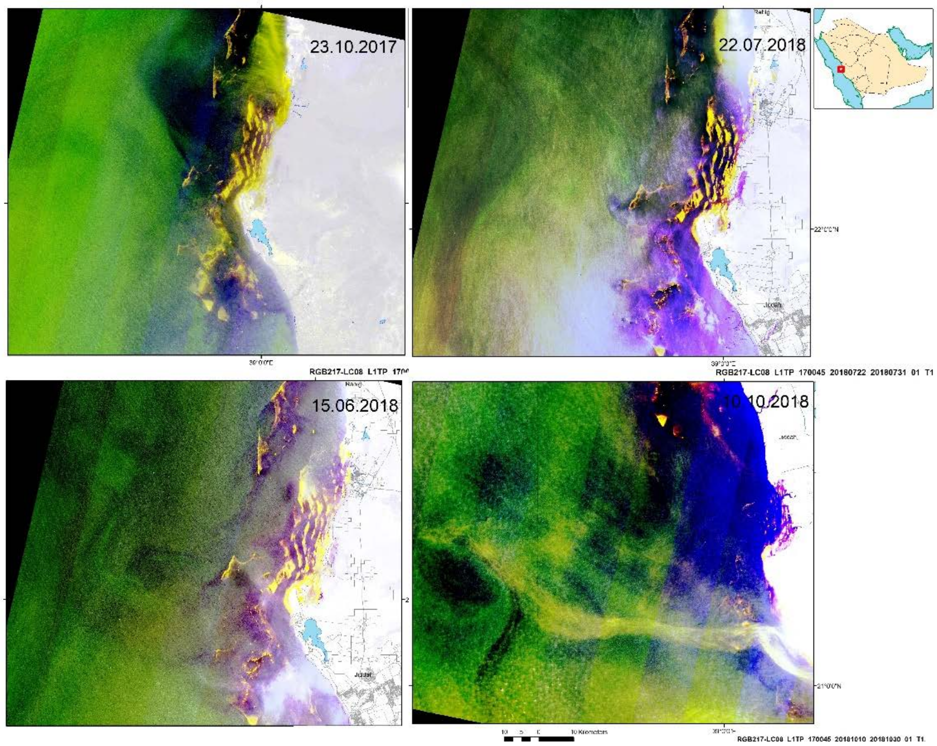

Figure 21. Different streaming and wave patterns at the coast of Jeddah visible on Landsat 8-scenes (RGB, Bands 2,1,7). On the scene of 10.10.2018, the sediment input of a dust storm is visible as a yellow band.

The bathymetric situation has an influence on the streaming pattern as well. Figure 22 visualizes the bathymetric contour lines on the Landsat 8-scene and, thus, showing the difference in the streaming pattern visible on the satellite image from deeper areas to flat shelf areas.

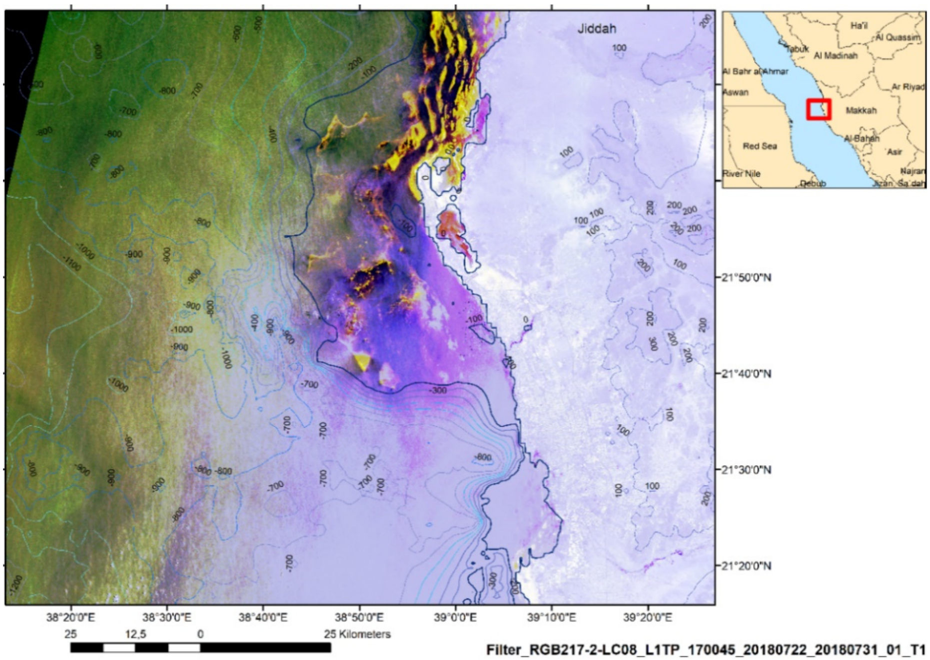

Figure 22. Streaming pattern near Jeddah influenced by the submarine topography (see bathymetric contour lines) and the morphology of islands.

When analysing the coastal morphology and General Bathymetric Chart of the Oceans (GEBCO) bathymetric data deeper, submarine valleys/canyons can be observed that are partly oriented perpendicular towards the coast (white arrows in Figure 23). In case of high energetic flood waves, such as tsunami waves caused by earthquakes, volcanic eruptions or submarine mass movements in the Red Sea the tsunami wave energies might be focused and concentrated along these valleys and, thus, in this case increasing the flooding extent in those coast segments.

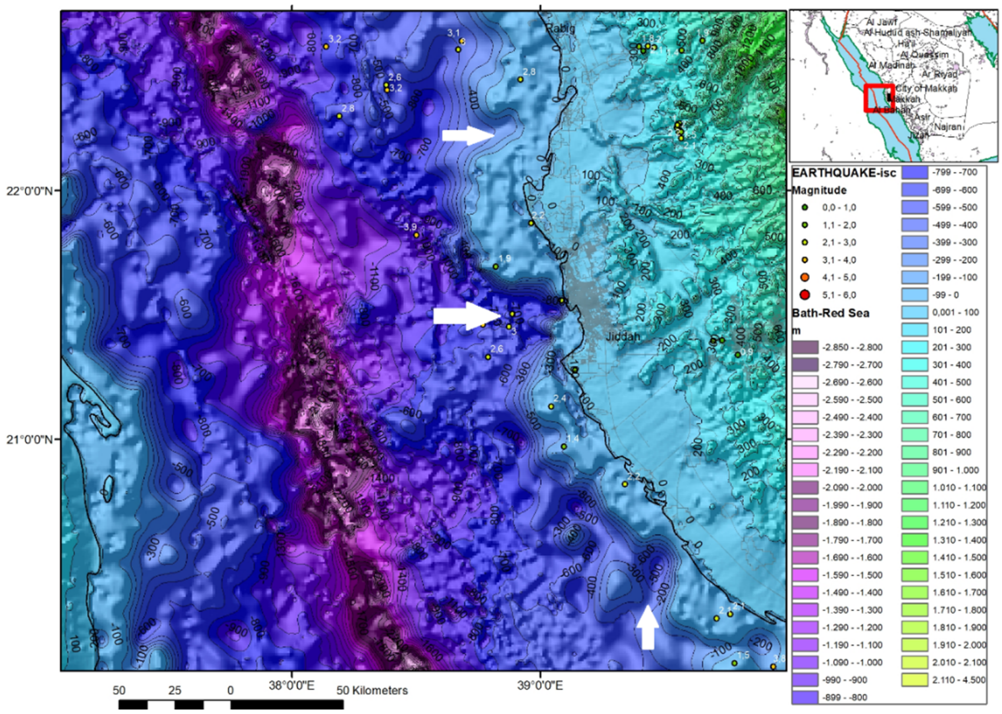

Figure 23. Submarine valleys near the coast with a potential focus of high energetic flood waves, such as tsunami waves. The map was created based on GEBCO bathymetric data.

6. Discussion

The examples of the use of remote sensing and GIS tools for the monitoring of natural hazards have shown that the continuously, systematic documentation and surveillance based on satellite data is a prerequisite not only for emergency preparedness, but also for the preparation of effective fieldwork.

Observations, such as geologic features like traces of compression or ring structures, need further investigations. The evaluation of the satellite data helps to focus this research. For example, the analysis of the different satellite data allows the detection of structural features in the subsurface, such as faults and ring structures more detailed than represented so far in geologic maps or even not visible in the field, due to younger sedimentary covers. Their specific origin and tectonic role should be investigated.

Landsat and Sentinel 1 and 2-data are an important tool for the water streaming observations in the Red Sea. When carried out in a regular pattern (of course combined with available in situ measurements), remote sensing data help to get more detailed knowledge about the complex factors influencing the current pattern in the Red Sea. This input will be important when dealing with storm surge or tsunami events as the interactions of meteo-tsunamis or tsunami waves with the local submarine and coastal morphologic conditions are still in investigation.

Preparedness and damage mitigation could be supported by creating DEM based maps indicating those areas that are prone to flooding, due to their geomorphologic disposition, especially in the coastal areas of Western Saudi Arabia. An example of the possible procedure was given of the region of Jeddah. Whenever a flash flood occurs in this area, its lowest and flattest parts are most likely to be affected. Land-use planning and protection measurements could be enhanced based on those kinds of maps that could be elaborated by every community without costs (data and software like SNAP from ESA and QGIS are free), if the necessary training of the staff is provided.

7. Conclusions

The combination of the evaluation results based on satellite images and digital elevation data of Western Saudi Arabia proved to be effective as input for geo-hazard assessment and natural hazard datamining. More detailed, and partly new, knowledge could be derived from the structural analysis of the remote sensing data.

Prevention of damage related to natural hazards (such as extreme rainfall or earthquakes and resulting secondary effects) to human life and infrastructure in Saudi Arabia requires preparedness and mitigation measurements that should be based on a regularly updated, GIS integrated data mining in order to create a data bank for the different geohazards. Remote sensing and GIS tools help to document changes after single natural hazard events and long-term changes as well, thus, forming a database for comparisons.

Like in other countries building up standardized information systems like in Indonesia the creation of standard structures and formats (describing the data, explain and synchronize data, use and management of data and its related contents) is a long-term process [42]. To produce accurate data that is up-to-date, GIS integrated, reliable, and easily accessible and shared between central and local agencies takes time. Therefore, a regularly, comparative analysis of satellite data will be an important part of such a database as the frequent coverage of free available data, such as Sentinel, Aster and Landsat are fundamental for this continuously updated monitoring and the necessary data storage of the natural hazards in Saudi Arabia [43] (Supplementary Materials). The standardized approach should be developed and adapted to the specific conditions and problems in this area. The expected more frequent extreme weather events and long-term modifications, due to climate change have to be taken into consideration as well.

Evaluations of the different satellite data from W-Saudi Arabia in the scope of this study contribute to the identification of areas prone to geohazards, to the detection of the different types of hazards and of some of the causal factors influencing the disposition to the specific hazards. With regard to the development of a natural hazard database adapted to the specific setting in Saudi Arabia the hereby presented examples might provide an idea of the input into workflows related to effective operation of disaster risk assessment and management. The quality in sensor and web design and data flow will continue to improve and, thus, facilitate its development. The shown examples may support the decisions about the procedures for a standardized natural hazard monitoring in this area.

Supplementary Materials: The following material is available online at http://www.mdpi.com/2076-3263/9/9/380/s1, Conference Contribution: Natural Hazard Assessment in Western Saudi Arabia using Remote Sensing and GIS Methods [43].

Author Contributions: Conceptualization, B.T.-W.; methodology, B.T.-W.; software, B.T.-W.; validation, B.T.-W. and H.W.; formal analysis, B.T.-W. and H.W.; investigation, B.T.-W.; resources, B.T.-W. and H.W.; writing—original draft preparation, B.T.-W.; writing—review and editing, B.T.-W.; visualization, B.T.-W.; supervision, H.W.; project administration, H.W.; funding acquisition, H.W.

Funding: This research received no external funding.

Acknowledgments: The authors are grateful for the input of the reviewers.

Conflicts of Interest: The authors declare no conflict of interest.

References

1. Al-Bassam, A.M.; Zaidi, F.K.; Hussein, M.T. Natural hazards in Saudi Arabia. In *Extreme Natural Hazards, Disaster Risks and Societal Implications*; Ismail-Zadeh, A., Urrutia-Fucugauchi, J., Kijko, A., Zaliapin, I., Eds.; Cambridge University Press: Cambridge, UK, 2014; pp. 243–251. Available online: https://fac.ksu.edu.sa/sites/default/files/enhans.pdf (accessed on 14 October 2018).
2. Centre for Research on the Epidemiology of Disasters (CRED). EM-DAT Database. Available online: https://www.emdat.be/database (accessed on 3 June 2018).
3. Intergovernmental Panel on Climate Change (IPCC). IPCC Fifth Assessment Report (AR5), Observed Climate Change Impacts Database, Version 2.01. Available online: https://doi.org/10.7927/H4FT8J0 (accessed on 3 October 2018).
4. National Oceanic and Atmospheric Administration (NOAA). Available online: https://maps.ngdc.noaa.gov/viewers/hazards/?layers=0 (accessed on 27 August 2019).
5. Bhuvan, Gateway to Indian Earth Observation. Available online: https://bhuvan-app1.nrsc.gov.in/bhuvandisaster/ (accessed on 27 August 2019).
6. Sentinel Asia. Available online: https://sentinel.tksc.jaxa.jp/sentinel2/topControl.jsp (accessed on 27 August 2019).
7. Van Westen, C.J. Remote sensing and GIS for natural hazards assessment and disaster risk management. *Treatise Geomorph.* **2013**, *3*, 259–298. [CrossRef]
8. Saudi Geological Survey (SGS), National Centre for and Volcanoes, Earthquake Seismology: Tectonics of the Arabian Plate. Available online: https://www.sgs.org.sa/English/Mobile/NaturalHazards/pages/geohazard.aspx (accessed on 25 October 2018).
9. Vescoukis, V.; Charalampos Bratsas, C. *Open Data in Natural Hazards Management*; Topic Report No: 2014/01; European Public Sector Information Platform (ePSIplatform): Brussels, Belgium, January 2014.
10. Youssef, A.M.; Maerz, N.H. Overview of some geological hazards in the Saudi Arabia. *Environ. Earth Sci.* **2013**, *70*, 3115–3130. [CrossRef]
11. Al-Ghamdi, K.; Elzahrany, R.A.; Mirza, M.N.; Gomaa, M.; Dawod, G.M. Impacts of urban growth on flood hazards in Makkah City, Saudi Arabia. *Int. J. Water Res. Environ. Eng.* **2012**, *4*, 23–34. [CrossRef]
12. Adams, R.D.; Barazangi, M. Seismotectonics And Seismology in The Arab Region: A Brief Summary and Future Plans. *Bull. Seismol. Soc. Am.* **1984**, *74*, 1011–1030.
13. Sakr, K.; Abdel-Monem, S.M.; Khalil, H.; Mahmoud, S.; Hamimi, Z.; Al-Aydrus, A.; Al Subary, A.; Al-Kottbah, A.; El Ganad, I.; Al-Gabary, A.; et al. A Study of Crustal Deformation along the Red Sea Region using Geodetic and Seismic Data from Egypt and Yemen. *Acta Geophys. Pol.* **2005**, *53*, 75–85.
14. Ligi, M.; Bonatti, E.; Tontini, F.C.; Cipriani, A.; Cocchi, L.; Schettino, A.; Bortoluzzi, G.; Ferrante, V.; Khalil, S.; Mitchel, N.C.; et al. Initial burst of oceanic crust accretion in the Red Sea due to edge driven mantle convection. *Geology* **2011**, *39*, 1019–1022. [CrossRef]
15. El-Isa, Z.H.; Al Shanti, A. Seismicity and tectonics of the Red Sea and western Arabia. *Geophys. J. Int.* **1989**, *97*, 449–457. [CrossRef]

16. Kassema, O.M.K.; Hamimi, Z. Finite Strain Analysis of the Wadi Fatima Shear Zone in Western Arabia, Saudi Arabia. *Geotectonics* **2018**, *52*, 251–265. Available online: https://www.researchgate.net/publication/327944832_Finite_Strain_Analysis_of_the_Wadi_Fatima_Shear_Zone_in_Western_Arabia_Saudi_Arabia_1 (accessed on 27 August 2019). [CrossRef]
17. US Geological Survey (USGS). Available online: https://earthquake.usgs.gov/earthquakes/search/ (accessed on 12 October 2018).
18. International Seismological Centre (ISC). *International Seismological Centre, On-Line Bulletin*; International Seismological Centre: Thatcham, UK, 2018.
19. European-Mediterranean Seismological Centre (EMSC). Available online: https://www.emsc-csem.org/#2 (accessed on 27 August 2019).
20. Smithsonian Institution's Global Volcanism Program (GVP). Eruptions, Earthquakes & Emissions, v. 1.0 (Internet Application). Available online: https://volcano.si.edu/E3/ (accessed on 25 January 2019).
21. Moufti, M.R.; Nemeth, K.; Murci, H.; Lindsay, J.M. The 1256 AD Al Madinah historic eruption geosite as the youngest volcanic chain in the Kingdom of Saudi Arabia. *Int. J. Earth Sci. (Geol. Rundsch.)* **2013**, *102*, 1069–1070. [CrossRef]
22. Pallister, J.S.; McCausland, W.A.; Jónsson, S.; Lu, Z.; Zahran, H.M.; El Hadidy, S.; Aburukbah, A.; Stewart, I.C.F.; Lundgren, P.R.; White, R.A.; et al. Broad accommodation of rift-related extension recorded by dyke intrusion in Saudi Arabia. *Nat. Geosci.* **2010**, *3*, 705–712. [CrossRef]
23. Xu, W.; Jónsson, S.; Corbi, F.; Rivalta, E. Graben formation and dike arrest during the 2009 Harrat Lunayyir dike intrusion in Saudi Arabia: Insights from InSAR, stress calculations and analog experiments. *J. Geophys. Res. Solid Earth* **2016**, *121*, 2837–2851. [CrossRef]
24. Camp, V.E.; Hooper, P.R.; Roobol, M.J.; White, D.L. The Madinah eruption, Saudi Arabia: Magma mixing and simultaneous extrusion of three basaltic chemical types. *Bull. Volcanol.* **1987**, *49*, 489–508. [CrossRef]
25. Jordan, B.R. Tsunamis of the Arabian Peninsula - A Guide of Historic Events. *Sci. Tsunami Hazards* **2008**, *27*, 31–46.
26. National Oceanic and Atmospheric Administration (NOAA). Global Historical Tsunami Database. Available online: https://www.ngdc.noaa.gov/hazard/tsu_db.shtml (accessed on 27 August 2019). [CrossRef]
27. General Bathymetric Chart of the Oceans (GEBCO), GEBCO's Gridded Bathymetric Data Set. Available online: https://www.gebco.net/data_and_products/gridded_bathymetry_data/ (accessed on 27 August 2019).
28. NOAA. Available online: https://oceanservice.noaa.gov/facts/seiche.html (accessed on 2 June 2018).
29. Youssef, A.M.; Pradhan, B.; Al-Kathery, M.; Bathrellos, G.D.; Skilodimou, H.D. Assessment of rockfall hazard at Al-Noor Mountain, Makkah city (Saudi Arabia) using spatio-temporal remote sensing data and field investigation. *J. Afr. Earth Sci.* **2015**, *101*, 309–321. [CrossRef]
30. Abdelkarim, A.; Gaber, A.F.D.; Youssef, A.M.; Pradhan, B. Flood Hazard Assessment of the Urban Area of Tabuk City, Kingdom of Saudi Arabia by Integrating Spatial-Based Hydrologic and Hydrodynamic Modeling. *Sensors* **2019**, *19*, 1024. [CrossRef] [PubMed]
31. Elkhrachy, I. Flash Flood Hazard Mapping Using Satellite Images and GI-Tools: A case study of Najran City, Kingdom of Saudi Arabia (KSA). *Egypt. J. Remote Sens. Space Sci.* **2015**, *18*, 261–278. [CrossRef]
32. Theilen-Willige, B.; Charif, A.; Chaïbi, M.; Ait Malek, H. Flash Floods in the Guelmim Area/SW-Morocco—Use of Remote Sensing and GIS-Tools for the Detection of Flooding Prone Areas. *Geosciences* **2015**, *5*, 203–221. [CrossRef]
33. Theilen-Willige, B.; Savvaidis, P.; Tziavos, I.N.; Papadopoulou, I. Remote Sensing and Geographi Information Systems (GIS) Contribution to the Inventory of Infrastructure Susceptible to Earthquake and Flooding Hazards in North-Eastern Greece. *Geosciences* **2012**, *2*, 203–220. [CrossRef]
34. USGS. Earth Explorer. Available online: https://earthexplorer.usgs.gov/ (accessed on 28 August 2019).
35. Alaska Satellite Facility (ASF). JAXA/METI, Accessed through ASF DAAC. Available online: https://www.asf.alaska.edu/ (accessed on 14 November 2018).
36. OpenStreetMap Data Extracts. Available online: http://download.geofabrik.de/ (accessed on 25 September 2018).
37. Fnais, M.; Amri, A.A.; Abdelrahman, K.; Abdelmonem, E.; El-Hady, S. Seismicity and Seismotectonics of Jeddah-Makkah Region, West-Central Saudi Arabia. *J. Earth Sci.* **2015**, *26*, 746–754. [CrossRef]

38. ArRajehi, A.; McClusky, S.; Reilinger, R.; Daoud, M.; Alchalbi, A.; Ergintav, S.; Gomez, F.; Sholan, J.; Bou-Rabee, F.; Ogubazghi, G.; et al. Geodetic constraints on present-day motion of the Arabian Plate: Implications for Red Sea and Gulf of Aden rifting. *Tectonics* **2010**, *29*, 1–10. [CrossRef]
39. Hamimi, Z.; Matsah, M.; El-Shafei, M.; El-Fakharani, A.; Shujoon, A.; Al-Gabali, M. Wadi Fatima Thin-Skinned Foreland FAT Belt: A Post Amalgamation Marine Basin in the Arabian Shield. *Open J. Geol.* **2012**, *2*, 271–293. [CrossRef]
40. Downs, D.T.; Stelten, M.E.; Champion, D.E.; Dietterich, H.R.; Nawab, Z.; Zahran, H.; Hassan, K.; Shawali, J. Volcanic history of the northernmost part of the Harrat Rahat volcanic field, Saudi Arabia. *Geosphere* **2018**, *14*, 1253–1282. [CrossRef]
41. Daoudi, M.; Niang, A.J. Flood Risk and Vulnerability of Jeddah City, Saudi Arabia. In *Recent Advances in Flood Risk Management*; IntechOpen: London, UK, 2019.
42. Abidin, H.Z. Status and Future Plans One Map Policy Indonesia. In Proceedings of the 15th South East Asia Survey Congress, Darwin, Australia, 15–18 August 2019.
43. Theilen-Willige, B.; Wenzel, H. Natural Hazard Assessment in Western Saudi Arabia using Remote Sensing and GIS Methods. Proceedings of the 2nd International Electronic Conference on Geoscience, 8–15 June 2019; Section: Earth Sciences through Earth Observation. Available online: https://sciforum.net/paper/view/6218 (accessed on 31 August 2019).